

# MULTIMODAL INTERPRETATION OF REMOTE SENSING IMAGES: DYNAMIC RESOLUTION INPUT STRATEGY AND MULTI-SCALE VISION–LANGUAGE ALIGNMENT MECHANISM

**Siyu Zhang**

School of Information Science and Technology  
Sanda University  
Shanghai 201209, China  
f23016217@st.sandau.edu.cn

Lianlei Shan

Tsinghua University  
Beijing 100084, China  
shanglianlei18@mails.ucas.edu.cn

**Ying Chen**

School of Information Science and Technology  
Sanda University  
Shanghai 201209, China  
ychen@sandau.edu.cn

Runhe Qiu\*

School of Information Science and Technology  
Sanda University  
Shanghai 201209, China  
qiurh@sandau.edu.cn

## ABSTRACT

Multimodal fusion of remote sensing images serves as a core technology for overcoming the limitations of single-source data and improving the accuracy of surface information extraction, which exhibits significant application value in fields such as environmental monitoring and urban planning. To address the deficiencies of existing methods, including the failure of fixed resolutions to balance efficiency and detail, as well as the lack of semantic hierarchy in single-scale alignment, this study proposes a Vision-language Model (VLM) framework integrated with two key innovations: the Dynamic Resolution Input Strategy (DRIS) and the Multi-scale Vision–language Alignment Mechanism (MS-VLAM). Specifically, the DRIS adopts a coarse-to-fine approach to adaptively allocate computational resources according to the complexity of image content, thereby preserving key fine-grained features while reducing redundant computational overhead. The MS-VLAM constructs a three-tier alignment mechanism covering object, local-region and global levels, which systematically captures cross-modal semantic consistency and alleviates issues of semantic misalignment and granularity imbalance. Experimental results on the RS-GPT4V dataset demonstrate that the proposed framework significantly improves the accuracy of semantic understanding and computational efficiency in tasks including image captioning and cross-modal retrieval. Compared with conventional methods, it achieves superior performance in evaluation metrics such as BLEU-4 and CIDEr for image captioning, as well as R@10 for cross-modal retrieval. This technical framework provides a novel approach for constructing efficient and robust multimodal remote sensing systems, laying a theoretical foundation and offering technical guidance for the engineering application of intelligent remote sensing interpretation.

## 1 INTRODUCTION

### 1.1 RESEARCH SIGNIFICANCE OF THE SUBJECT

Remote sensing (RS) imagery, acquired via satellite-borne or airborne sensors, serves as a pivotal technology for capturing geospatial information of the Earth’s surface [1]. Endowed with inherent advantages including extensive coverage, high spatiotemporal resolution, and rich spectral characteristics, RS has become an indispensable tool across diverse domains such as environmental

\*Corresponding author. E-mail: qiurh@sandau.edu.cn

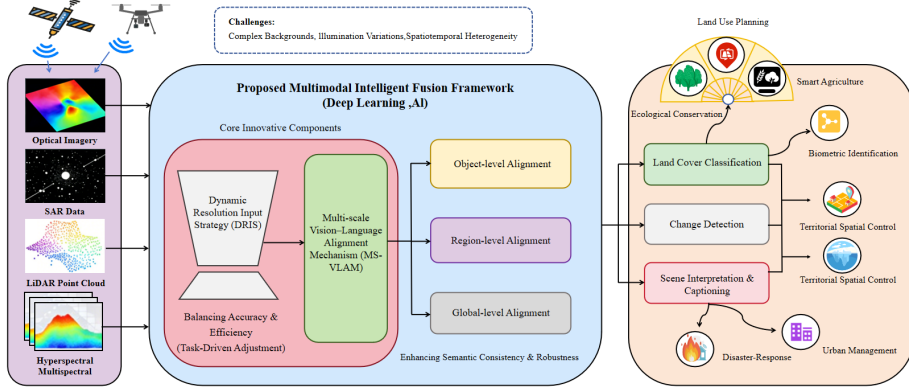


Figure 1: Overview of the proposed multimodal intelligent fusion framework for remote sensing applications. The framework first processes multi-source remote sensing data (optical imagery, SAR, LiDAR, hyperspectral) via the **Dynamic Resolution Input Strategy (DRIS)**, which balances feature extraction accuracy and computational efficiency. Cross-modal semantic matching is then implemented through the **Multi-scale Vision–language Alignment Mechanism (MS-VLAM)**, which decomposes alignment into Object-level, Local-region-level, and Global-level granularities to strengthen visual-textual consistency. This framework supports a variety of downstream tasks, including land cover classification, disaster response, and urban management.

monitoring, urban planning, agricultural surveying, and disaster assessment [2, 3]. With the continuous advancements in imaging and sensing technologies, RS data have evolved from traditional unimodal optical imagery to multimodal and multisource formats, encompassing synthetic aperture radar (SAR), light detection and ranging (LiDAR), multispectral, and hyperspectral imagery. This evolution has significantly enhanced the comprehensiveness and granularity of Earth observation, enabling more precise and holistic characterization of surface features [4, 5, 6].

However, remote sensing (RS) imagery still confronts multiple technical bottlenecks in practical deployment: including complex background clutter, subtle inter-class discrepancies among land cover types, and significant time-varying fluctuations in illumination and meteorological conditions. Such inherent complexities have substantially constrained the performance of precise information extraction and high-level semantic interpretation tasks for RS data[7]. In this context, multimodal comprehensive understanding techniques offer a forward-looking technical pathway to address these challenges by fusing structural features, temporal dynamic patterns, and spatial correlations encapsulated in heterogeneous sensor data. This approach can effectively overcome the inherent limitations of unimodal RS analysis, enabling robust execution of high-level tasks (e.g., land cover classification, change detection, and scene semantic interpretation) and significantly improving the accuracy and reliability of intelligent RS imagery analysis[8, 9].

With the rapid advancement of deep learning and artificial intelligence technologies, a comprehensive multimodal understanding of RS imagery has emerged as a key frontier research direction in the contemporary RS domain[10]. On one aspect, constructing a unified multimodal data fusion framework enables both complementary information integration across heterogeneous data sources and effective suppression of uncertainties and noise perturbations associated with single-source data dependence, thus markedly improving the accuracy and robustness of land surface parameter retrieval and information extraction[11]. On the other aspect, to address practical challenges (e.g., strong spatiotemporal heterogeneity of RS data and scarcity of annotated samples), exploring emerging methodological paradigms (including self-supervised learning, cross-domain transfer learning, and graph neural networks) holds critical theoretical guidance and practical support value for enhancing model generalization and adaptability, as well as facilitating the large-scale deployment of multimodal RS technologies[12, 13, 14].

In this context, this study presents two core innovations: a task-driven Dynamic Resolution Input Strategy (DRIS) and a Multi-scale Vision–language Alignment Mechanism (MS-VLAM). The former adaptively tunes the input image resolution based on task specifications and computational

---

constraints, striking a balance between high analytical accuracy and computational efficiency. This attribute makes it particularly tailored to RS scenarios characterized by ultra-wide coverage and coexisting multi-scale features. The latter realizes cross-modal feature semantic alignment at the Object, Local-region, and Global levels, which markedly enhances the robustness and precision of cross-modal retrieval, object detection, and semantic interpretation for RS data[15]. This integrated design effectively alleviates the challenges of granularity inconsistency and semantic misalignment in multimodal fusion, thereby offering a novel paradigm for building an efficient and scalable RS multimodal understanding system.

The advancement of multimodal comprehensive understanding technologies embodies not only substantial academic value but also broad prospects for practical and strategic applications. It facilitates the transition of RS data toward in-depth intelligent interpretation, driving technological progress in domains such as ecological conservation, smart agriculture, urban planning, and disaster response[16]. Specifically, in ecological and environmental conservation, multimodal fusion technologies enable more accurate monitoring of forest cover dynamics, wetland degradation processes, and water resource conditions (aligning with the framework’s ecological conservation application)[17]; in smart agriculture, they support dynamic crop growth monitoring and precise detection of pests and diseases[18]; in urban management, they assist in land use planning and surveillance of urban expansion (supporting land use planning and urban planning tasks)[19]; and in disaster response, they enhance rapid response and assessment capabilities for hazards including earthquakes, floods, and wildfires[20].

Moreover, international cutting-edge research trends in remote sensing (RS) indicate that multimodal fusion-driven intelligent analysis is progressing toward three pivotal directions: large-scale spatiotemporal data processing (for global-scale Earth observation), cross-domain knowledge transfer (to mitigate data disparities across distinct RS scenarios), and multi-task joint learning (to unify heterogeneous downstream tasks)[21, 22, 23]. By harnessing integrated cloud-edge computing architectures, which integrate low-latency edge inference and large-capacity cloud storage, this paradigm enables real-time processing and on-demand updating of high-throughput RS data streams[24]. This capability directly overcomes the efficiency bottleneck of conventional RS information services, thereby further elevating the intelligence and automation of application-centric remote sensing service systems, e.g., those for regional ecological monitoring or emergency disaster response[25].

In summary, research on multimodal comprehensive understanding of RS imagery is not only an inevitable requirement for the innovation and theoretical advancement of remote sensing technology but also a strategic initiative to address the demand for high-quality geospatial information services in the intelligent era. By providing theoretical guidance and technical support for constructing efficient and robust RS information processing systems, this research will contribute to the realization of Digital Earth and Smart Earth visions, while facilitating leapfrog development in geographic information science and related application domains[16, 26].

## 1.2 PREVIOUS METHODS AND SHORTCOMINGS

As a core underpinning of visual-language understanding, the cross-modal alignment mechanism between vision and language has garnered extensive attention and in-depth exploration in recent years [27]. Existing methodologies primarily achieve cross-modal semantic matching between remote sensing (RS) imagery and text through feature representation learning and similarity measurement, yet they suffer from inherent limitations in two core technical aspects that hinder their performance in complex RS scenarios.

On the one hand, conventional RS image feature extraction methodologies predominantly rely on fixed-resolution input strategies [28]. Specifically, most models normalize all input images to a pre-defined resolution to ensure consistent dimensions for batch processing and model training. Nevertheless, this paradigm exhibits notable drawbacks: high-resolution inputs preserve abundant fine-grained details but substantially augment computational overhead and GPU memory consumption, compromising the efficiency of both training and inference; in contrast, low-resolution inputs reduce computational costs but often lead to the loss of critical fine-scale visual information, impairing the model’s ability to perceive local details and thus undermining its performance in understanding complex RS scenes. Furthermore, the uniform fixed-resolution processing lacks flexibility

---

to dynamically allocate computational resources according to the inherent complexity of RS images, ultimately restricting the model’s generalization across diverse RS visual interpretation tasks.

On the other hand, existing RS cross-modal alignment approaches primarily rely on object-level or global-level strategies to establish correspondences between RS imagery and textual descriptions [29]. Early research focused predominantly on global alignment, which matches the holistic features of an entire RS image with the comprehensive semantic features of a complete text passage[30]. While this paradigm captures overall inter-modal semantic consistency, it overlooks inherent fine-grained semantic associations within both RS imagery and text , resulting in inadequate comprehension of specific ground objects or local scene details. Subsequent studies have attempted to integrate local feature alignment methods (e.g., region-based object detection bounding boxes or fragment-level feature representations) to enhance the matching accuracy between individual ground objects or local image regions and their corresponding textual elements[31]. However, most current approaches remain confined to object-level alignment, lacking systematic multi-scale semantic modeling capabilities that would enable simultaneous capture of semantic consistency across object-level, local-region-level, and global-level level. Moreover, object-level alignment often disregards the multi-layered semantic hierarchies inherent in both visual (RS imagery) and textual modalities, constraining the expressive power of cross-modal associations and rendering these methods ill-equipped for complex RS tasks demanding fine-grained semantic understanding and contextual reasoning, such as RS image-text retrieval and visual question answering.

Beyond the aforementioned limitations, the majority of current RS cross-modal methods lack hierarchical structure in their overall feature representations [32], which hinders the effective capture of structured information regarding interrelationships among different ground objects, local regions, and their contextual associations. In complex RS scenes, ground objects typically exhibit specific spatial configurations, semantic correlations, and interactive relationships. These characteristics cannot be accurately depicted solely through flat and holistic feature descriptions. For advanced RS visual-language tasks (e.g., scene graph generation and multi-object interaction understanding), models require the ability to hierarchically recognize and represent distinct ground objects while capturing their positional, action, and causal relationships [33]. The single-level representation limitation of current methods restricts in-depth understanding and reasoning of inter-object relationships and semantic interactions in complex scenarios, failing to meet the requirements for high-level RS visual-language reasoning.

Additionally, the trade-off between computational efficiency and alignment accuracy remains a prominent challenge for RS cross-modal alignment methods. Achieving finer-grained semantic alignment generally necessitates processing high-resolution image inputs and conducting complex multi-scale feature computations, leading to substantial consumption of computational resources and increased latency during both training and inference phases[34]. This constraint impairs the scalability and real-time performance of such methods in practical RS applications; particularly in large-scale RS datasets and real-time monitoring scenarios, the excessive computational burden becomes a critical bottleneck restricting the widespread deployment and adoption of cross-modal alignment models [35].

In summary, existing RS vision-language alignment methods exhibit notable deficiencies across four interrelated aspects: inadequate fixed-resolution handling strategies that fail to balance efficiency and detail preservation [36]; insufficient multi-scale alignment paradigms that overlook inherent multi-layered semantic structures [37]; inadequate hierarchical modeling of complex ground objects and their interactive relationships [38]; and excessive computational resource demands that limit practical deployment [39]. To address these critical bottlenecks, it is essential to develop a cross-modal alignment framework that integrates dynamic resolution input processing with systematic multi-scale alignment. This framework specifically incorporates object-level, local-region-level, and global-level cross-modal visual-language alignment mechanisms, and it will serve as a key breakthrough for advancing high-performance visual-language understanding in RS.

### 1.3 OUR APPROACH AND GAINS OBTAINED

To address the aforementioned limitations, this paper presents a novel instantiation of the proposed cross-modal alignment framework. This framework is specifically designed to tackle the dual chal-

---

lenges of resolution efficiency and scale adaptability (derived from the deficiencies outlined earlier) through two core innovations:

- Innovation 1: Dynamic Resolution Input Strategy(DRIS)

Traditional methods typically process images at a fixed resolution, making it difficult to flexibly accommodate visual information of varying granularity, which results in significant GPU memory consumption and computational load, while also limiting efficient analysis of large-scale regions. To overcome this bottleneck, this paper introduces a dynamic resolution input strategy(DRIS), employing a coarse-to-fine multi-stage processing strategy: the model first captures global semantic context at a reduced resolution to ensure computational efficiency. It then adaptively increases the resolution to focus on high-priority regions and extract finer visual features, thereby effectively balancing computational efficiency and expressive capability.

- Innovation 2: Multi-scale Vision–language Alignment Mechanism(MS-VLAM)

Current remote sensing (RS) cross-modal alignment methods primarily rely on object-level or global-level feature matching, neglecting the correspondence between visual features and textual features across multiple semantic granularity levels. This approach struggles to fully capture cross-modal associations in complex remote sensing scenarios. To address this gap, this paper proposes a multi-scale vision-language alignment mechanism that systematically models the hierarchical matching relationship between visual regions in remote sensing imagery and textual semantics. This mechanism enhances both the granularity of remote sensing image and text understanding while strengthening the overall consistency of cross-modal representations. Specifically, the mechanism encompasses the following three levels:

**Object-level Alignment:** This level targets the correspondence between individual ground objects in RS imagery (e.g., “mountain ridge,” “vegetation patch”) and their lexical or phrasal descriptors in text. It is implemented via object detection, bounding box feature extraction, and cross-modal alignment between image patch embeddings and text token representations. This fine-grained alignment enhances the model’s capacity to associate specific RS visual entities with textual referents, thereby improving its sensitivity to concrete semantic elements in scene descriptions.

**Local-region-level Alignment:** This level targets the semantic correspondence between localized regions in RS imagery (e.g., “rocky outcrops on grassland,” “valley edge”) and textual phrases or clauses. It achieves this by aggregating adjacent image patch features or pooling region-level representations, which aligns local visual context in RS scenes with textual fragments. This process enables the capture of inter-object spatial relationships, local scene structures, and composite semantic information inherent to complex remote sensing environments.

**Global-level Alignment:** This level targets the alignment between the entire RS imagery and full text segments, with the goal of capturing semantic consistency between the overall scene context and the complete textual narrative. This alignment preserves thematic coherence and contextual background consistency between the remote sensing image and text, thereby enhancing the model’s capacity to interpret complex narratives and multi-component scene contexts in remote sensing applications.

In summary, the proposed dynamic resolution input module and multi-scale vision-language alignment mechanism, through synergistic design, specifically address the critical limitations of existing methods in resolution efficiency and scale adaptability. The DRIS module optimises computational efficiency while preserving fine-grained visual information, whereas the Multi-scale Vision–language Alignment Mechanism(MS-VLAM) effectively enhances cross-modal semantic capture across hierarchical granularities. Their synergistic interaction markedly enhances the model’s overall performance in remote sensing visual-language tasks, achieving an efficient equilibrium between computational efficiency and feature representation capability. This integrated framework not only provides crucial theoretical underpinnings for cross-modal representation learning in remote sensing but also demonstrates outstanding practical value in real-world applications involving the comprehension of complex remote sensing scenarios.

---

#### 1.4 CONTRIBUTION SUMMARY

As outlined earlier, existing RS vision-language cross-modal alignment methods face four interrelated limitations: (1) fixed-resolution input pipelines that cannot balance computational efficiency and fine-detail preservation; (2) single-scale alignment paradigms that overlook multi-layered semantic structures; (3) insufficient hierarchical modeling of ground object interactions; and (4) excessive computational costs that restrict practical deployment. To mitigate these bottlenecks, this paper makes four targeted contributions:

- **Proposing a dynamic resolution input strategy (addressing Limitation 1):** This mechanism dynamically adjusts input resolution based on RS image content complexity. It reduces computational overhead while preserving critical fine-grained visual information, resolving the efficiency-detail trade-off in fixed-resolution pipelines and enhancing the model’s detail-capturing capability for complex RS scenes.
- **Designing a systematic multi-scale vision–language alignment mechanism (addressing Limitation 2):** A hierarchical alignment strategy (spanning object-level, local-region-level, and global-level) is developed. This strategy enables joint modeling and consistent alignment of cross-modal features across semantic granularities, effectively capturing multi-layered RS data semantics and boosting the model’s expressive power in tasks like vision-language retrieval.
- **Introducing a hierarchical structure-aware mechanism (addressing Limitation 3):** To model spatial layouts, semantic associations, and interactions among RS ground objects, a structured representation method is designed. This method captures positional relationships, action correlations, and contextual links, supporting structured reasoning for tasks such as scene graph generation.
- **Achieving efficient high-precision alignment (addressing Limitation 4):** The integrated framework alleviates the efficiency-accuracy trade-off in cross-modal alignment. It improves alignment precision and scene adaptability while ensuring scalability and real-time performance, overcoming computational barriers to practical deployment in large-scale RS applications.

Collectively, the proposed dynamic resolution input strategy and multi-scale vision–language alignment mechanism offer a cohesive solution to the four core limitations of existing methods. It provides theoretical insights and practical support for advancing high-performance cross-modal visual-language understanding in real-world remote sensing scenarios.

## 2 RELATED WORK

### 2.1 SEGMENTATION OF REMOTE SENSING IMAGES

Remote sensing (RS) image segmentation serves as a foundational step in intelligent RS scene interpretation. Its core objective is to partition complex RS scenes into semantically homogeneous regions and extract target object information, thereby supporting diverse downstream applications including urban planning, crop growth monitoring, and natural disaster assessment [40]. This section systematically reviews the evolutionary landscape of RS image segmentation methods, ranging from traditional techniques to state-of-the-art deep learning-based approaches, while clarifying key technical advancements, inherent limitations, and critical research gaps.

Traditional RS image segmentation techniques were the earliest research focus, encompassing thresholding, edge detection, region growing and merging, graph-based algorithms (e.g., Graph Cut, Normalized Cut), and object-based image analysis (OBIA) [41]. These methods rely on handcrafted features such as pixel intensity, texture, and edge contours, and exhibit advantages of algorithmic simplicity, high computational efficiency, and strong interpretability. However, their performance degrades significantly when processing high-resolution RS imagery with complex backgrounds or multi-class objects, often leading to over-segmentation or under-segmentation artifacts. A fundamental limitation lies in their inability to effectively model contextual information and spatial structural relationships between objects.

---

With the advancement of machine learning, RS image segmentation gradually shifted toward learning-based paradigms [42]. Representative methods include Support Vector Machines (SVM), Random Forests (RF), and clustering algorithms such as K-means and Fuzzy C-Means (FCM). These approaches reformulate segmentation as a pixel-level or object-level classification task, leveraging engineered spectral, texture, and shape features for discrimination. While they achieve improved segmentation accuracy in small-sample scenarios, these methods still depend heavily on labor-intensive manual feature engineering. Moreover, they lack the capability to automatically extract high-level semantic features, limiting their performance in capturing complex spatial contextual relationships within RS scenes.

In recent years, deep learning-based methods have emerged as the dominant paradigm in RS image segmentation, driving substantial improvements in segmentation accuracy and spatial structure preservation. The Fully Convolutional Network (FCN) pioneered this field by replacing fully connected layers in traditional convolutional neural networks with convolutional layers, enabling end-to-end pixel-level segmentation and supporting input images of arbitrary sizes [43]. Despite this breakthrough, FCN suffers from severe spatial detail loss during successive downsampling operations, resulting in blurred segmentation boundaries that are unacceptable for high-precision RS applications.

To address the limitations of FCN, U-Net and its variants have been widely adopted in RS image segmentation tasks. U-Net employs a symmetric encoder-decoder architecture, where the encoder extracts hierarchical features through downsampling and the decoder recovers spatial resolution via upsampling. Skip connections between corresponding encoder and decoder layers effectively fuse shallow fine-grained features with deep high-level semantic features, thus preserving boundary details and spatial information [44]. To adapt to the complex shapes and irregular distributions of ground objects in RS imagery, improved architectures such as Attention U-Net, ResU-Net, and Nested U-Net (U-Net++) have been proposed. These variants integrate attention mechanisms, residual connections, and dense connections to enhance the model's capability in segmenting small objects and handling complex RS scenes [45].

The DeepLab series represents another pivotal branch of deep learning-based RS segmentation methods, with DeepLabV3 and DeepLabV3+ being the most influential variants [46]. Their core innovations include Atrous Convolution and Atrous Spatial Pyramid Pooling (ASPP), which expand the receptive field of convolutional layers without increasing model parameters or computational costs. This design enables the model to capture multi-scale contextual information, making it suitable for segmenting RS targets of varying sizes [47]. In addition, DeepLabV3+ incorporates an encoder-decoder structure to further refine spatial details and adopts Conditional Random Fields (CRF) as a post-processing step to optimize boundary representations, significantly improving segmentation accuracy in complex RS scenes [48].

With the growing demand for global context modeling in large-scale RS imagery, Transformer-based architectures and their hybrid designs have been increasingly introduced into RS image segmentation. Transformers leverage self-attention mechanisms to capture long-range spatial dependencies and global semantic relationships, providing strong interpretability for complex RS scenes [49]. Typical examples include Swin Transformer, which adopts a hierarchical structure and sliding window self-attention to balance global information capture and computational efficiency [50]; SegFormer, which combines a lightweight Transformer encoder with a simple decoder to achieve high-accuracy and efficient segmentation [51]; and TransUNet, which embeds Transformer modules into the U-Net architecture to integrate the local feature extraction capability of CNNs with the global modeling power of Transformers, enabling accurate segmentation in complex backgrounds [52].

To further address the unique challenges of RS imagery, such as large target scale variations and blurred object boundaries, researchers have integrated a series of specialized enhancement techniques into deep learning models. Multi-scale feature fusion techniques including Feature Pyramid Networks (FPN), ASPP, and Pyramid Pooling Modules (PSPNet) are widely used to capture both local fine-grained details and global contextual information [53]. Attention mechanisms such as Squeeze-and-Excitation (SE) modules, Convolutional Block Attention Module (CBAM), and self-attention modules are employed to selectively enhance discriminative features, improving the model's sensitivity to small objects and boundary regions [54]. For the problem of limited labeled RS data, weakly supervised segmentation, self-supervised pretraining, and domain adaptation meth-

---

ods have been explored to reduce reliance on large-scale annotated datasets and enhance cross-region generalization capability [55].

Beyond single-modal and single-scale methods, multi-modal and multi-scale fusion approaches have been proposed to further boost segmentation performance for complex RS scenes. Multi-modal methods integrate complementary data sources such as optical imagery, Synthetic Aperture Radar (SAR) data, and LiDAR elevation data, performing fusion at the feature level, decision level, or joint embedding space to enhance the model’s discriminative ability in heterogeneous backgrounds [56]. Multi-scale methods adopt strategies including image pyramids, FPN, atrous convolutions, and ASPP to handle the scale diversity of RS targets, effectively addressing the low segmentation accuracy of small objects and large-scale scenes [57]. Additionally, Graph Neural Networks (GNNs) have been incorporated into RS segmentation by constructing spatial graph structures at the pixel or superpixel level, modeling spatial contextual relationships through node adjacency, and further improving segmentation completeness and accuracy [3].

## 2.2 DATA ANALYSIS OF REMOTE SENSING IMAGES

The remote sensing image data employed in this experiment originates from the large-scale multi-modal remote sensing dataset created by the MBZUAI team for constructing the GeoChat model. This dataset is specifically designed to address the training and evaluation requirements of Large Vision-language Models in remote sensing scenarios. It aims to resolve the issue of inadequate adaptability of general-purpose vision-language datasets in the remote sensing domain, providing high-quality annotated support for cross-modal understanding tasks involving remote sensing imagery. The dataset focuses on the characteristics of high-resolution remote sensing imagery, covering diverse remote sensing scenarios including urban built-up areas, farmland, mountainous forested regions, water bodies and wetlands, transport hubs, and industrial zones. It incorporates remote sensing imagery from various sensors (such as optical satellites and UAVs), different shooting angles, and temporal sequences, ensuring broad data distribution and representativeness. At the annotation level, the dataset incorporates not only image-level and local-region-level semantic descriptions but also multi-task annotation information such as Visual Question Answering and referential object detection. This forms a tripartite multimodal annotation system encompassing ‘image-text-region’, providing rich supervisory signals for fine-grained understanding and cross-modal reasoning of remote sensing imagery.

To align with experimental requirements, a tailored preprocessing workflow was designed based on the raw GeoChat dataset to ensure data quality and model input compatibility. During the data screening and cleaning phase: 1. Relevant remote sensing images and associated annotations were selected based on specific research scenarios (e.g., ‘urban land classification,’ ‘transportation facility identification’), excluding irrelevant scenarios to effectively reduce noise interference; Subsequently, quality validation was conducted to eliminate image samples exhibiting blurring, excessive cloud cover, or substandard resolution (below the experiment’s specified resolution threshold). Concurrently, annotation data integrity and consistency were meticulously verified, removing samples with missing annotations or semantic conflicts to safeguard data reliability at source.

During image preprocessing, a uniform resizing strategy addresses dimensional variations in remote sensing imagery. All filtered images are adjusted to a fixed, predefined experimental resolution (e.g., 224×224, 512×512), employing bilinear interpolation to preserve image detail and prevent distortion during scaling. To address potential issues such as uneven illumination and variations in grey-scale distribution within remote sensing images, standardisation processing is applied. By calculating the mean and standard deviation of the dataset’s pixels, image pixel values are transformed into a distribution range compliant with model training requirements, thereby mitigating the impact of extraneous factors like illumination on experimental outcomes. Furthermore, for annotated data, the original annotation formats (e.g., JSON, XML) are converted into input formats supported by the experimental models. Regional annotations undergo coordinate calibration to ensure precise alignment between annotation information and image pixel locations, establishing a robust data foundation for subsequent model training and evaluation.

Regarding data partitioning and evaluation design, to guarantee experimental objectivity and reliability, a stratified random partitioning strategy is employed. The preprocessed dataset is divided into training, validation, and test sets at a ratio of [7:2:1]. During partitioning, the distribution

---

of samples across different scenarios and task types within each dataset is maintained consistent with the original dataset, thereby preventing model evaluation distortion caused by data partitioning bias. Furthermore, leveraging the multi-task nature of the GeoChat dataset, corresponding evaluation metrics were established for core experimental tasks (e.g., remote sensing image captioning, visual question answering, scene classification). Classification and detection tasks were assessed using accuracy, precision, recall, and F1 score, while image description tasks employed metrics such as BLEU, ROUGE, and CIDEr for image description tasks, comprehensively measuring model performance across remote sensing image analysis tasks.

### 2.3 MULTIMODAL UNDERSTANDING OF REMOTE SENSING IMAGES

With the rapid advancement of remote sensing technology, the types and volumes of acquired remote sensing data have expanded explosively, covering optical imagery, Synthetic Aperture Radar (SAR) images, LiDAR point cloud data, hyperspectral images, and datasets from diverse sensors and platforms. These data sources vary in spatial resolution, spectral information, temporal frequency, and imaging principles, but each carries inherent limitations: optical imagery is susceptible to weather and lighting interference; SAR can penetrate clouds and precipitation yet lacks fine spatial resolution and texture details[58]; LiDAR provides high-precision 3D terrain information but involves complex processing and higher costs[59]. Thus, multimodal remote sensing image understanding, which fuses multi-source, multi-dimensional data, can fully leverage the complementary advantages of each modality, enabling more comprehensive and accurate object recognition and information extraction.

Current multimodal fusion techniques are primarily divided into three levels:

**Pixel-level fusion:** Aligns and combines data from different modalities at the pixel level to generate composite images containing multimodal information, laying a data foundation for subsequent analysis[16]. However, this method requires high spatial alignment accuracy and is typically used for image enhancement and composite feature extraction.

**Feature-level fusion:** First extracts features independently from each modality, then concatenates or weights these feature vectors[60]. In recent years, deep learning approaches (e.g., multi-branch networks, attention mechanisms, cross-modal transformers) have been widely applied here to explore inter-modal relationships and enhance feature representation[16].

**Decision-level fusion:** Performs classification or detection separately on each modality, then integrates results via weighting, voting, or rule-based strategies[61]. This approach is simple and flexible, but its performance largely depends on the quality of individual single-modal models.

While multimodal remote sensing understanding has advanced significantly, it still faces core challenges:

**Data heterogeneity:** Differences in spatial resolution, sampling rates, and noise characteristics across modalities make high-precision registration and alignment a fundamental hurdle.

**Information redundancy conflict:** Data from different modalities may overlap or contradict, requiring effective fusion mechanisms to retain complementary information while filtering irrelevant or interfering content.

**Efficient processing:** Massive remote sensing datasets (especially high-resolution temporal multimodal data) pose critical demands for efficient processing and real-time analysis.

**Model generalization:** Data distributions vary sharply across regions and environments, so enhancing the adaptability of multimodal fusion models in complex scenarios is key to their practical application.

In recent years, deep learning has driven progress in this field: CNN-based multi-branch architectures extract features from each modality separately, then enable information interaction via fusion layers[52]; attention-based methods dynamically adjust modality weights to focus on key regions and critical features[50]; Transformer-based multimodal architectures effectively model long-range inter-modal dependencies, boosting feature richness and robustness[56]. These methods have promoted multimodal remote sensing applications in land use classification, urban planning, disaster

monitoring (e.g., floods, fires), environmental protection, and agricultural assessment, supporting intelligent management across related industries.

In the future, as remote sensing data accumulates and computational technologies advance, multimodal remote sensing fusion is expected to move toward greater intelligence, automation, and real-time processing. By integrating big data analytics, cloud computing, and artificial intelligence, it will elevate remote sensing information services, providing robust technical support for Earth observation, sustainable development, and emergency management[62].

### 3 METHODS

#### 3.1 OVERVIEW OF METHODS: VISUAL-LANGUAGE MODEL (VLM)

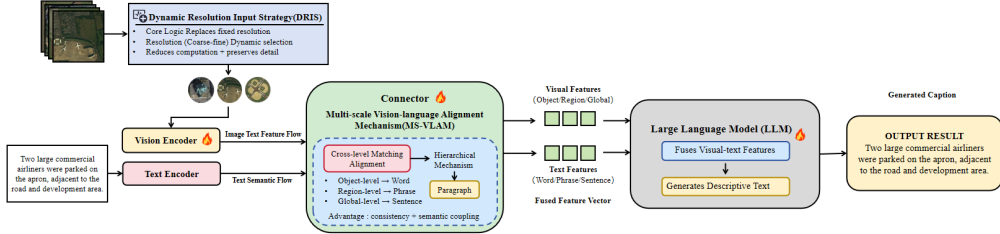


Figure 2: Workflow of the dynamic resolution visual-language fusion framework for remote sensing image captioning. This framework integrates a coarse-to-fine dynamic resolution input strategy (balancing computational efficiency and detail preservation), a multi-scale visual-text alignment module (matching object, local-region, global visual features with textual units), and a hierarchical fusion module. The fused visual-linguistic features are fed into a large language model (LLM) to generate semantically consistent descriptive captions (e.g., “Two large commercial airliners were parked on the apron”).

This study constructs a VLM for image semantic modeling and natural language generation (see Figure 2). The framework consists of four core components: a Vision Encoder, a Connector module, a Text Encoder, and a Large Language Model (LLM). In its baseline workflow, the Vision Encoder first extracts semantic features from input images. The Connector then transforms these features into vector representations compatible with language models. Concurrently, the Text Encoder embeds input text such as task instructions and contextual prompts into semantic vectors. Finally, the fused vision-language features are fed into the LLM to generate descriptive outputs such as image captions. This architecture enables efficient alignment and deep integration of visual-textual information, with strong generalizability for tasks including image captioning, visual question answering, and multimodal reasoning.

However, in complex remote sensing scenes, the baseline model still faces two key challenges, namely, scale inconsistency and imprecise vision-language alignment. To this end, based on the baseline VLM, this study enhances the visual encoder and connector module, aiming to improve the scene adaptability and cross-modal understanding ability of the model through these two improvements.

#### 3.2 DYNAMIC RESOLUTION INPUT STRATEGY(DRIS)

In remote sensing scenarios, the DRIS flexibly adjusts the input image resolution during inference or training, significantly reducing computational and memory overhead while maintaining accuracy. Remote sensing images often have large spatial coverage, high resolution, and complex land-cover structures; directly using a fixed high-resolution input not only imposes substantial GPU memory and computational costs but also limits the capability for rapid analysis of large areas. The Dynamic Resolution Input method typically employs a coarse-to-fine strategy, which can be formalized mathematically as a dynamic resolution allocation function:

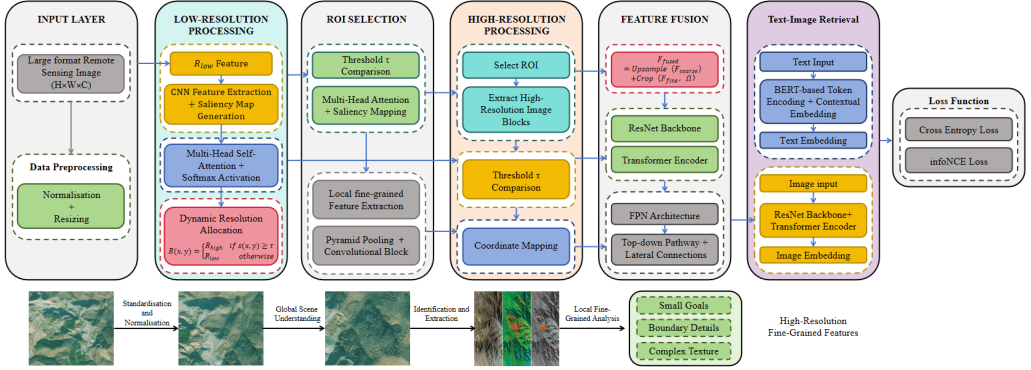


Figure 3: The workflow of the proposed high-resolution remote sensing fine-grained processing framework. Starting from large-format remote sensing image input (after preprocessing), the pipeline first extracts low-resolution features and saliency maps, then selects regions of interest (ROIs) via threshold comparison and attention-based saliency mapping. High-resolution processing refines ROI blocks, followed by feature fusion using a ResNet-Transformer-FPN architecture. Finally, vision-language retrieval is implemented with BERT text embedding and ResNet image embedding, optimized by cross entropy and infoNCE losses. The bottom illustration visualizes the stepwise refinement from global scene understanding to local fine-grained analysis (e.g., small object/boundary detail extraction).

$$R(x, y) = \begin{cases} R_{\text{high}} & \text{if } s(x, y) \geq \tau \\ R_{\text{low}} & \text{otherwise} \end{cases} \quad (1)$$

where  $R(x, y)$  denotes the output value  $R$  at the point  $(x, y)$ ; the regional significance score  $s(x, y)$  is obtained through the global analysis in the low-resolution stage, and  $\tau$  is the adjustable threshold; when the condition  $s(x, y) \geq \tau$  is established, the function returns the value  $R_{\text{high}}$ , otherwise it returns the value  $R_{\text{low}}$ .

The mechanism first conducts low-resolution processing of large-format remote sensing images  $R_{\text{low}}$ , to quickly complete the scene understanding, coarse-grained target detection and regional localization, in order to quickly screen the region of interest (Region of Interest, ROI), at this time, the computational complexity is only for the high-resolution processing of the  $\frac{1}{n^2}$  ( $n$  is the down-sampling times); subsequently, the identification of the target region or the change of the sensitive region to extract high-resolution image block, at this time, the system is only for the target region that meets the requirements of. Subsequently, high-resolution image blocks are extracted from the identified target area or change-sensitive area, at this time, the system only enables high-resolution ( $R_{\text{high}}$ ) analysis of the region of interest (ROI) that meets the requirements of  $s(x, y) \geq \tau$ , and carries out local fine-grained analysis and fine segmentation to realize the accurate capture of small targets, boundary details and complex textures.

To achieve effective integration of multi-scale features during the Dynamic Resolution Input process, the model framework incorporates a Feature Pyramid Network (FPN) fusion strategy. Let the low-resolution feature map be  $F_{\text{coarse}}$  and the high-resolution localized features be  $F_{\text{fine}}$ , then the fusion process is expressed as:

$$F_{\text{fused}} = \text{Upsample}(F_{\text{coarse}}) + \text{Crop}(F_{\text{fine}}, \Omega) \quad (2)$$

where  $F_{\text{fused}}$  denotes the final output variables and results of the feature map,  $\Omega$  denotes the ROI spatial range,  $\text{Upsample}(\cdot)$  denotes the up-sampling of a certain feature map to make its size compatible with the subsequent operations, and  $\text{Crop}(\cdot)$  denotes the cropping of a certain feature map

---

to make its size aligned with the up-sampled feature map to ensure that both of them are spatially aligned with each other in terms of features.

In addition, the attention mechanism is introduced into the dynamic resolution processing framework to enhance the screening efficiency of ROIs and further improve the model’s ability to detect and characterize targets at different scales. Firstly, the attention heatmap  $A_{\text{coarse}}$  is computed in the low-resolution stage, and then Gaussian filtering is used to smooth out the noise and select the most significant region of Top-K, and the final output of ROI screening efficiency  $P_{\text{ROI}}$ , the mathematical expression of which can be formalized as:

$$P_{\text{ROI}} = \text{Topk}(\text{GaussianBlur}(A_{\text{coarse}}), k) \quad (3)$$

where  $A_{\text{coarse}} \in \mathbb{R}^{\frac{H}{n} \times \frac{W}{n}}$  represents the coarse-grained attention heatmap generated in the low-resolution processing stage,  $H$  and  $W$  represent the height and width of the original image, respectively, and  $n$  is the downsampling factor; the Gaussian smoothing operator  $\text{GaussianBlur}(\cdot)$  represents the preprocessing of the heatmap, and the value of the standard deviation  $\sigma$  is usually set to 1.5-2.0 in order to balance the noise suppression and the edge preservation; the  $\text{Topk}(\cdot)$  selection operation represents the selection of the top  $k$  regions with the highest response values from the processed heatmap as the candidate ROIs.

In large-scale remote sensing intelligent analysis, DRIS not only reduces redundant computation and improves inference efficiency and throughput — addressing the precision-efficiency trade-off in fine-grained analysis for complex scenarios — but also provides a practical pathway for large-scale intelligent remote sensing tasks in geographic information analysis, urban management, and environmental monitoring. This strategy lays a lightweight, efficient foundation for the subsequent multi-scale vision-language alignment (Section 3.3).

### 3.3 MULTI-SCALE VISION-LANGUAGE ALIGNMENT MECHANISM (MS-VLAM)

This section presents the multi-scale vision language alignment mechanism (MS-VLAM), which is designed to balance fine-grained local feature mining and global semantic coherence for complex scenes. The framework enforces alignment constraints across three hierarchical scales including object, local-region, and global image, and realizes adaptive optimization of downstream tasks through weighted loss fusion and joint training.

In cross-level vision language analysis tasks, the MS-VLAM framework dynamically adjusts the weights of three scale specific alignment losses (Object level Alignment Loss, Local-region level Alignment Loss, Global level Alignment Loss) based on image content features, ensuring optimized performance for both simple descriptive tasks and fine-grained reasoning tasks. Within a single task, the framework captures increasingly precise semantic details as the alignment scale refines, which strengthens fine-grained semantic parsing and achieves comprehensive high-fidelity vision language semantic alignment.

Concretely, the framework first extracts visual representations of salient objects via a detector and ROI pooling, then aligns these representations with entity level text features. Concurrently, it adopts the Segment Anything Model (SAM) or a comparable region segmentation method to generate semantically consistent local regions, which are further matched to phrase level embeddings (PhraseEmbed). Finally, multi-scale global semantic representations are derived using Spatial Pyramid Pooling (SPP) and aligned with the CLS or global vector of the full text. To guarantee training stability and alignment robustness, task appropriate strategies are deployed at each scale: dynamic IoU based weighting is applied for object level alignment, soft matching or contrastive learning is adopted for region level alignment, and norm normalized projection is employed for global level alignment.

#### 3.3.1 SINGLE-OBJECT SCALE-DEPENDENT LOSS FUNCTION

At the single object scale, we first extract visual features from the  $p^{\text{th}}$  candidate frame (output by detectors such as Faster R-CNN or DETR) via ROI pooling and ROIAlign, then project these features into the alignment space. The visual feature vector  $\mathbf{v}_{\text{obj}}^{(p)}$  of the  $p^{\text{th}}$  aligned candidate frame is defined as:

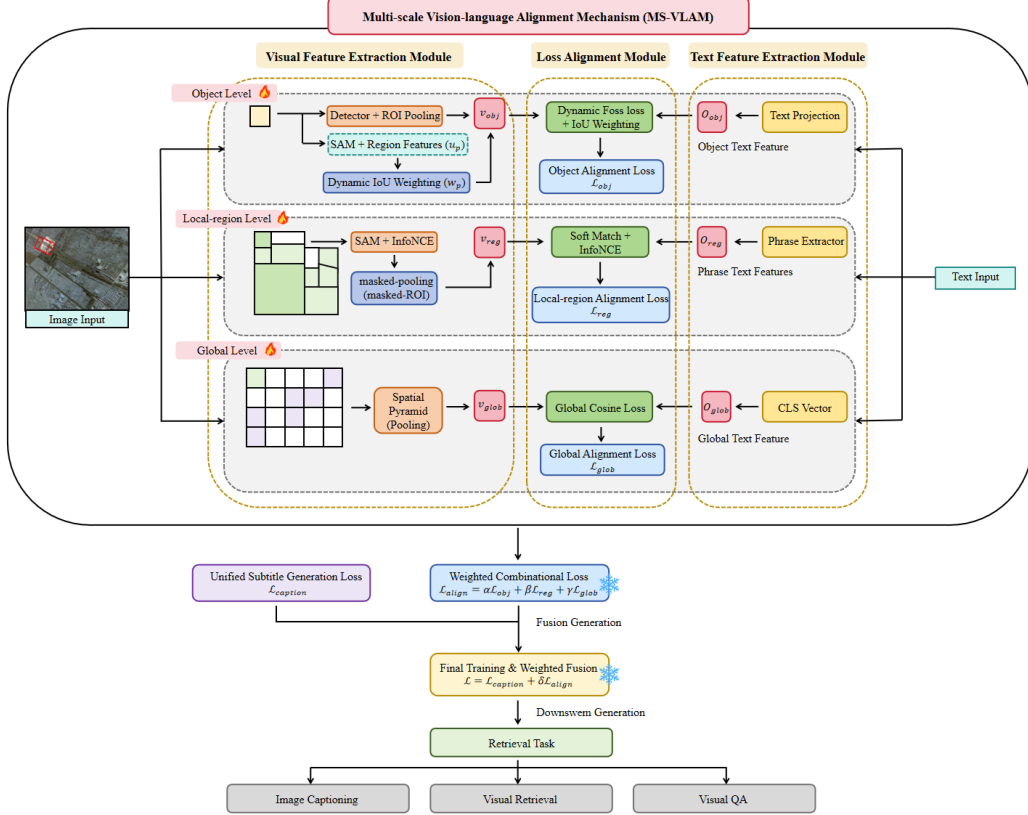


Figure 4: The framework of Multi-scale Vision-language Alignment Mechanism (MS-VLAM). This framework comprises three core modules. First, the Visual Feature Extraction Module extracts visual features at three scales: object-level features via detector and ROI pooling, local-region-level features via SAM-based segmentation and masked pooling, and global-level features via spatial pyramid pooling. Second, the Text Feature Extraction Module generates corresponding text features from the text input, including object text features, phrase text features, and global CLS vector features. Third, the Loss Alignment Module conducts scale-specific vision-language alignment and calculates alignment losses for each scale. Finally, the weighted combinational loss (fused with the captioning loss) is applied to optimize the model, supporting downstream tasks such as image captioning, visual retrieval, and visual QA.

---


$$\mathbf{v}_{\text{obj}}^{(p)} = f_{\text{v}}(\text{RoI}(V, \mathbf{B}_p)) \quad (4)$$

where  $V$  denotes the overall visual features of the input image;  $\mathbf{B}_p$  denotes that the  $p^{\text{th}}$  candidate frame is generated by a detector (e.g., Faster R-CNN or DETR); RoI denotes the shorthand of RoI Pooling or RoI Align, which is used to extract the local area features corresponding to the candidate frame  $\mathbf{B}_p$  from the image features  $V$ ; and  $f_{\text{v}}(\cdot)$  denotes the projection function (usually a fully-connected layer or a linear transformation) that maps the RoI-extracted features to the alignment space. The function formulation is able to convert the candidate box region features output by the detector into a vector representation comparable to the text features. The corresponding text entity is projected to the entity description (or entity label) by the text encoder to obtain the aligned feature vector of the text entity, which is represented by the function  $\mathbf{o}_{\text{obj}}^{(p)}$ :

$$\mathbf{o}_{\text{obj}}^{(p)} = f_{\text{t}}(\mathbf{e}_p) \quad (5)$$

where  $\mathbf{e}_p$  denotes the original representation of the text entity (e.g., object category label or descriptive text);  $f_{\text{t}}(\cdot)$  denotes the text projection function, which maps the text features to the same alignment space as the visual features. This function formula can convert text information into vectors with the same dimension as visual features, which is convenient for subsequent similarity calculation.

In order to directly measure the semantic similarity between visual and text, it is calculated using the cosine similarity formula, whose function  $\cos(\mathbf{u}, \mathbf{v})$  is denoted as:

$$\cos(\mathbf{u}, \mathbf{v}) = \frac{\mathbf{u}^{\top} \mathbf{v}}{\|\mathbf{u}\| \|\mathbf{v}\|} \quad (6)$$

where  $\mathbf{u}^{\top} \mathbf{v}$  denotes the matrix representation of the dot product (inner product) of vectors  $\mathbf{u}$  and  $\mathbf{v}$  ( $\mathbf{u}$  transposed and multiplied by  $\mathbf{v}$ ); and  $\|\mathbf{u}\| \|\mathbf{v}\|$  denotes the Euclidean norm (modulus length) of the vector.

Considering the importance of the quality of the detection frame for alignment, we improve the traditional single-object alignment loss function by introducing dynamic IoU-based weighting coefficients for each object, and do normalization to avoid numerical instability, so that the model can adaptively focus on object instances that are more accurately localized. The improved object-level alignment loss function  $\mathcal{L}_{\text{obj}}$  is:

$$\mathcal{L}_{\text{obj}} = 1 - \frac{1}{P} \sum_{p=1}^P w_p \cdot \cos(\mathbf{v}_{\text{obj}}^{(p)}, \mathbf{o}_{\text{obj}}^{(p)}) \quad (7)$$

where  $P$  is the number of object instances;  $\mathbf{v}_{\text{obj}}^{(p)}$  denotes the visual feature of the  $p^{\text{th}}$  object;  $\mathbf{o}_{\text{obj}}^{(p)}$  denotes the text feature corresponding to the object;  $w_p$  are weighting coefficients, which are dynamically computed from the IoU of the predicted frame and the real frame:

$$w_p = \frac{\text{IoU}(\hat{\mathbf{B}}_p, \mathbf{B}_p)}{\sum_{q=1}^P \text{IoU}(\hat{\mathbf{B}}_p, \mathbf{B}_q)}$$

This mechanism can strengthen the contribution of objects with higher localization accuracy in the loss computation, thus improving the stability of fine-grained semantic alignment.

### 3.3.2 LOCAL-REGIONAL-LEVEL LOSS FUNCTION

At the local-region scale, we innovatively propose the local-region aggregation alignment method. A set of semantic masks or segmented regions generated by Segment Anything Model (SAM) is used as a set of candidate regions  $\{\mathbf{R}_k\}_{k=1}^K$ , where  $K$  is the number of semantic regions. Each region undergoes masked-pooling or masked-RoI operation to get the region visual features  $\mathbf{v}_k$ .

---

Corresponding to the text side, the phrase extractor generates the set of phrases that may correspond to the semantics of the region  $\{t_j\}_{j=1}^M$ , where  $M$  is the number of text regions. And mapped to vector  $\mathbf{p}_j = \text{PhraseEmbed}(t_j)$  using PhraseEmbed module. Since regions and phrases are often one-to-many or many-to-one relationships and direct one-to-one correspondence may not be robust, we adopt two types of complementary strategies at the local-region level: first, region-by-region hard-match aggregation loss for easier interpretation; and second, region-phrase intercomparison learning (InfoNCE) to learn soft-match distributions. The hard match aggregation loss function  $\mathcal{L}_{\text{reg}}^{\text{hard}}$  is denoted as:

$$\mathcal{L}_{\text{reg}}^{\text{hard}} = 1 - \frac{1}{K} \sum_{k=1}^K \cos(\mathbf{v}_k, \mathbf{p}_{\pi(k)}) \quad (8)$$

where  $\pi(k)$  denotes a human or heuristically selected phrase index. The contrast learning form first computes the similarity matrix, and its similarity matrix function  $s_{kj}$  can be expressed as:

$$s_{kj} = \frac{\mathbf{v}_k^\top \mathbf{p}_j}{\tau} \quad (9)$$

where  $\tau > 0$  denotes the temperature parameter. Then InfoNCE loss (anchored by region) is defined with soft match aggregation loss function:

$$\mathcal{L}_{\text{reg}}^{\text{NCE}} = -\frac{1}{K} \sum_{k=1}^K \log \frac{\exp(s_{k,y(k)})}{\sum_{j=1}^M \exp(s_{kj})} \quad (10)$$

where  $y(k)$  denotes the positive sample phrase index of region  $k$ . Finally, we synthesize the local-region aggregation alignment loss in weighted combinatorial form, whose local-region aggregation alignment loss function  $\mathcal{L}_{\text{reg}}$  is denoted as:

$$\mathcal{L}_{\text{reg}} = \mu \mathcal{L}_{\text{reg}}^{\text{hard}} + (1 - \mu) \mathcal{L}_{\text{reg}}^{\text{NCE}}, \quad \mu \in [0, 1] \quad (11)$$

This mechanism can effectively model the spatial relationship between objects and the semantic information of regions, and make up for the shortcomings of the traditional single-object alignment method when dealing with multi-object interactions.

### 3.3.3 GLOBAL-LEVEL SCALE LOSS FUNCTION

At the global scale, we extract the multi-scale convergent representation from the visual feature map  $V$  by introducing Spatial Pyramid Pooling (SPP). A common SPP structure is to do the average/maximum pooling of  $V$  with different resolutions such as  $1 \times 1$ ,  $2 \times 2$ ,  $4 \times 4$  and splice them together, and then obtain the global visual vector of uniform dimensions by linear transformation  $\mathbf{g} = \text{SPP}(V)$ , where  $\text{SPP}(V)$  denotes the global features of the image obtained by multi-scale pooling operation, which can capture the scene background and macro-contextual information at different spatial granularities to ensure the consistency between the visual content and the textual description at the macro-level. The CLS vector or sentence-level representation of the whole text  $t_{[\text{CLS}]}$  is used on the text side, and in order to ensure the synergy of scale information and numerical stability, layer normalization (LayerNorm) and L2 normalization are done after projection. The global scale alignment loss function  $\mathcal{L}_{\text{glob}}$  can be defined as:

$$\mathcal{L}_{\text{glob}} = 1 - \cos(\mathbf{g}, t_{[\text{CLS}]}) \quad (12)$$

In order to comprehensively coordinate the alignment contributions of the three scales, the final multiscale alignment objective function  $\mathcal{L}_{\text{align}}$  is defined in the form of weighted combination as:

$$\mathcal{L}_{\text{align}} = \alpha \cdot \mathcal{L}_{\text{obj}} + \beta \cdot \mathcal{L}_{\text{reg}} + \gamma \cdot \mathcal{L}_{\text{glob}} \quad (13)$$

where  $\alpha, \beta, \gamma$  are the weights of Object level, Local-region level, and Global level respectively, and satisfy  $\alpha, \beta, \gamma \geq 0$ , reflecting the focus on different granularity tasks.

---

### 3.4 LOSS FUNCTION AND OPTIMIZATION PROCESS

In order to enhance the visual-verbal alignment ability of the model at different scales while ensuring the overall semantic consistency, we add a unified subtitle generation loss  $\mathcal{L}_{\text{caption}}$  to the multi-scale alignment loss function  $\mathcal{L}_{\text{align}}$ . Given a sequence of subtitles corresponding to an input image  $(x_1, x_2, \dots, x_T)$ , the subtitle generation loss function  $\mathcal{L}_{\text{caption}}$  is defined as:

$$\mathcal{L}_{\text{caption}} = - \sum_{k=1}^K \log P_{\text{L}}(x_k | V, x_{<t}) \quad (14)$$

where  $V$  is the visual feature embedding, which can be visual information at single-object level, local-region level or global level, and  $P_{\text{L}}(\cdot)$  is the predicted probability based on visual and textual context. The loss-promoting model is able to generate text descriptions that are coherent and consistent with the visual content, reinforcing the correspondence between visual features and text semantics.

As part of the loss function design (the core of this section), the final training objective function is formulated as the weighted sum of the multi-scale alignment loss and the caption generation loss:

$$\mathcal{L} = \mathcal{L}_{\text{caption}} + \delta \cdot \mathcal{L}_{\text{align}} \quad (15)$$

where  $\delta > 0$  is an important hyperparameter to balance the two components. This joint training strategy integrates multi-scale vision-language alignment losses with caption generation loss, enabling the model not only to achieve precise alignment at the object, local-region, and global levels but also to learn holistic semantic representations through the text generation task. As a result, the model’s depth and breadth in vision-language understanding are significantly enhanced.

In terms of the optimization process, the model is implemented based on the PyTorch framework, with CUDA acceleration and bfloat16 mixed-precision training adopted to improve efficiency. The training configuration is set as follows: each batch processes 8 image-text pairs; the AdamW optimizer is used with an initial learning rate of  $3 \times 10^{-4}$ ; the learning rate undergoes a 100-step warmup phase, then linearly decays to 0 over 1000 total steps; for memory optimization, only the embedding parameters of the linear mapping layer and the special token [RET] are updated during training (other parameters remain frozen). During each iteration, the model computes the total loss first, then updates trainable parameters via backpropagation—this process enables effective multi-modal feature fusion and enhances the model’s text generation capability for remote sensing images.

## 4 EXPERIMENTS

### 4.1 INTRODUCTION TO THE DATASET

To comprehensively enhance the reasoning and understanding capabilities of vision-language models in remote sensing scenarios, this study utilizes the RS-GPT4V dataset. This dataset integrates multiple typical remote sensing vision-language subtasks, including Image Captioning, Visual Question Answering (VQA), Visual Grounding, Local-region-level Captioning, Multi-turn Conversation, and Detailed Description. Its sources cover publicly available datasets such as NWPU-Captions, RSICD, RSITMD, Sydney-Captions, UCM-Captions, RSVQA-LR, RSVQA-HR, Flood-Net, RSIVQA, and DIOR-RSVG, supplemented with the newly constructed RS-GPT4V-Instruct. This integration establishes a large-scale, multi-task, and multi-modal benchmark, providing a comprehensive evaluation platform for vision-language modeling in complex remote sensing scenes.

In terms of scale, the RS-GPT4V dataset contains 91,937 training images corresponding to 991,206 instruction-answer pairs, and a test set of 15,999 images with 258,419 instruction-answer pairs. These instruction-answer pairs not only cover conventional image captioning and question-answering tasks but also support local-region-level localization and description, as well as multi-turn interactions for complex dialogue scenarios.

With its diverse tasks and fine-grained annotations, the RS-GPT4V dataset supports research across multiple levels, including image-to-text generation, visual reasoning, and multi-turn dialogue modeling. It facilitates advances in remote sensing vision-language understanding and provides a solid experimental foundation for cross-modal reasoning and complex semantic analysis.

---

Compared with existing remote sensing vision-language datasets, RS-GPT4V offers the following notable advantages:

- **Task Diversity:** Traditional datasets often focus on a single task. For instance, RSICD and RSITMD primarily serve image captioning, while RSVQA is dedicated to visual question answering. RS-GPT4V, in contrast, provides a unified integration of multiple tasks, including image captioning, visual question answering, local-region-level grounding and description, multi-turn dialogue, and detailed descriptions, supporting a more comprehensive scope for multimodal research.
- **Larger Scale:** Compared with existing single-task datasets, which typically contain only thousands to tens of thousands of images or annotations, RS-GPT4V is significantly larger, comprising 91,937 training images with 991,206 instruction–answer pairs, and 15,999 test images with 258,419 instruction–answer pairs, representing an order-of-magnitude increase in dataset size.
- **Finer Annotation Granularity:** Most existing remote sensing datasets provide only coarse-grained annotations at the image or Q&A level. In contrast, RS-GPT4V supports not only image-level descriptions but also local-region-level visual grounding and detailed captions. Additionally, it incorporates multi-turn dialogue formats, enhancing the dataset’s capacity for complex semantic reasoning and contextual modeling.
- **Unified Benchmark Characteristics:** Existing studies often require separate experiments across multiple datasets, resulting in inconsistent task settings. RS-GPT4V integrates data from diverse tasks into a single unified benchmark, facilitating joint training and evaluation of models across multi-task scenarios.

In summary, compared with traditional remote sensing vision-language datasets, RS-GPT4V demonstrates significant advantages in task diversity, data scale, annotation granularity, and benchmark uniformity, providing stronger support for research and applications of multimodal models in the remote sensing domain.

## 4.2 IMPLEMENTATION DETAILS

In this study, a VLM based multimodal framework was tailored for remote sensing imagery to mitigate scale inconsistency and inaccurate vision-language alignment. This section elaborates on the framework’s architecture, multi-scale alignment mechanism (implementation of Eq. (13)), training configuration, and key advantages.

### 4.2.1 FRAMEWORK ARCHITECTURE

For input processing, remote sensing images were standardized to a resolution of  $224 \times 224 \times 3$  and partitioned into 196 non-overlapping patches of  $16 \times 16$  pixels; each patch was flattened into a vector and projected into a 768-dimensional feature space via a learnable linear layer. To preserve spatial positional information, a trainable positional embedding (`pos_embed`) with dimensions  $1 \times 196 \times 768$  was added to the patch features, and these augmented features were then fed into a 12-layer Transformer Encoder (12 attention heads per layer, hidden dimension = 768, feedforward network dimension = 3072), yielding the final image representation with shape  $(B, 196, 768)$  (where  $B$  denotes the batch size, set to 8 in this study).

Text inputs were first converted into 768-dimensional embeddings ( $\text{text}_{\text{feat}}$ ) via an embedding layer, resulting in a feature shape of  $(B, T, 768)$  (where  $T$  is the text sequence length, with a maximum truncation length of 64 tokens); in the Cross-Modal Attention module, text features served as Queries while image features acted as Keys and Values, and this module employed 12 attention heads (each with a dimension of 64) to compute the text-to-image attention distribution, with the attention output linearly projected to generate fused features ( $\text{fused}_{\text{feat}}$ ) that retained the shape  $(B, T, 768)$ .

The  $\text{fused}_{\text{feat}}$  was subsequently fed into a 12-layer Transformer Decoder (12 attention heads per layer, hidden dimension = 768, feedforward network dimension = 3072) for textual description generation, and the decoder output was finally linearly mapped to the vocabulary size (32,000) to

---

produce the predicted probability distribution  $y_{\text{pred}}$ , which was used for cross-entropy loss calculation.

#### 4.2.2 MULTI-SCALE VISION-LANGUAGE ALIGNMENT MECHANISM

To implement the Multi-scale Vision-language Alignment Mechanism (MS-VLAM) (Eq. (13) in Section 3.3), this framework integrates object-level, local-region-level, and global-level alignment into the training pipeline. Specifically, the  $\mathcal{L}_{\text{align}}$  (Eq. (13)) is realized by mapping visual features (from Section 4.2.1) to object level, local-region level, and global-level representations, then computing  $\mathcal{L}_{\text{obj}}$ ,  $\mathcal{L}_{\text{reg}}$ ,  $\mathcal{L}_{\text{glob}}$  via cross-modal similarity metrics between these visual representations and corresponding text embeddings.

During training, weights  $\alpha, \beta, \gamma$  are dynamically adjusted to balance the three loss components (synchronized with  $\delta$  in Eq. (15)). This implementation ensures the model captures fine-grained semantic correspondence across scales while maintaining training stability.

#### 4.2.3 TRAINING CONFIGURATION AND OPTIMIZATION

To implement the loss function (Eqs. (13)-(15)) and optimization strategy (Section 3.4), the model was built on the PyTorch framework with CUDA acceleration and bfloat16 mixed-precision training (to improve efficiency). The training configuration is set as follows: each batch processes 8 image-text pairs, the AdamW optimizer is used with an initial learning rate of  $3 \times 10^{-4}$ , the learning rate undergoes a 100-step warmup phase then linearly decays to 0 over 1000 total steps, and for memory optimization, only the parameters of the linear projection layer and the embeddings of the special token [RET] are updated during training (while other parameters remain frozen).

The experimental dataset is constructed using 1% of the HuggingFace COCO dataset (consisting of 1,000 images and their corresponding textual descriptions), and a custom collate function is employed for data preprocessing—including RGB conversion, resizing, and normalization for images, as well as tokenization, truncation, and padding for text sequences.

During each training iteration, the model first computes the total loss via the objective function defined in Eqs. (13)-(15), then updates the trainable parameters through backpropagation, followed by optimizer parameter updates and learning rate adjustment according to the scheduling strategy; this process enables effective multi-modal feature fusion and enhances the model’s text generation capability for remote sensing images.

#### 4.2.4 KEY IMPLEMENTATION ADVANTAGES

From an implementation perspective, this framework integrates dynamic resolution input and the multi-scale alignment mechanism (Section 4.2.2) to achieve precise semantic correspondence from the object level to the global level. In complex remote sensing scenarios, the implemented design enables the generation of accurate and coherent textual descriptions while balancing training efficiency and memory usage.

The tight integration of the Vision Encoder, Cross-Modal Attention module, and Language Decoder in the implementation ensures efficient multimodal understanding, which significantly enhances the model’s text generation and semantic comprehension performance for remote sensing imagery. Additionally, the framework’s implementation maintains high flexibility with clearly defined hyperparameter configurations and training strategies, facilitating reproducibility and further optimization in subsequent experiments.

### 4.3 EVALUATION INDICATORS

For performance evaluation in the image captioning task, this study adopts eight automatic evaluation metrics, namely BLEU-1, BLEU-2, BLEU-3, BLEU-4, METEOR, ROUGE-L, CIDEr, and SPICE. These metrics comprehensively quantify the quality of the generated text across multiple dimensions, including surface-level matching, semantic coverage, coherence, and informativeness.

---

The BLEU (Bilingual Evaluation Understudy) metric evaluates surface similarity by calculating the n-gram overlap between the generated text and the reference text. Its calculation formula is:

$$\text{BLEU-}N = \text{BP} \cdot \exp \left( \sum_{n=1}^N w_n \log p_n \right) \quad (16)$$

where  $p_n$  represents the n-gram precision, i.e., the proportion of n-grams in the generated text that match those in the reference text;  $w_n$  denotes the weight, which is usually distributed uniformly (i.e.,  $w_n = \frac{1}{N}$ ); and BP refers to the brevity penalty, defined as:

$$\text{BP} = \begin{cases} 1, & c > r \\ e^{1-\frac{r}{c}}, & c \leq r \end{cases} \quad (17)$$

where  $c$  denotes the length of the generated text and  $r$  denotes the length of the reference text. In the experiments, BLEU-1 to BLEU-4 correspond to unigram, bigram, trigram, and 4-gram matches, respectively, enabling a stepwise evaluation of surface matching quality from the word level to the phrase level.

The METEOR (Metric for Evaluation of Translation with Explicit ORdering) metric extends BLEU by incorporating stemming and synonym matching, thus providing a more flexible assessment of semantic correspondence. Its core formula is:

$$F_{\text{mean}} = \frac{10 \cdot P \cdot R}{R + 9P}, \quad \text{METEOR} = F_{\text{mean}} \cdot (1 - \text{Pen}) \quad (18)$$

where  $P$  and  $R$  denote the precision and recall between the generated text and the reference text, respectively. The fragmentation penalty (Pen) is applied to penalize discontinuous matching segments in the generated text. In METEOR, the weight assigned to recall is typically higher than that of precision, reflecting the importance of semantic coverage completeness in the generated text.

The ROUGE-L metric evaluates the coherence of the generated text based on the Longest Common Subsequence (LCS). Its precision, recall, and F1 score are defined as follows:

$$P_L = \frac{\text{LCS}(X, Y)}{|X|}, \quad R_L = \frac{\text{LCS}(X, Y)}{|Y|}, \quad F_1 = \frac{(1 + \beta^2) \cdot P_L \cdot R_L}{R_L + \beta^2 \cdot P_L} \quad (19)$$

where  $X$  and  $Y$  denote the generated text and the reference text, respectively, and  $\beta$  is usually set to 1 to balance the influence of precision and recall. ROUGE-L effectively reflects the structural integrity and fluency of the generated text.

The CIDEr (Consensus-based Image Description Evaluation) metric computes the consistency between the generated text and a set of reference descriptions using TF-IDF weighted similarity, emphasizing the informativeness of the text. Its formula is:

$$\text{CIDEr}_n(c_i, s_i) = \frac{1}{|S_i|} \sum_{s \in S_i} \frac{\mathbf{g}_n(c_i) \cdot \mathbf{g}_n(s_j)}{\|\mathbf{g}_n(c_i)\| \|\mathbf{g}_n(s_j)\|} \quad (20)$$

where  $\mathbf{g}_n(\cdot)$  represents the TF-IDF vector of n-grams, and  $S_i$  denotes the set of reference descriptions. Typically, 1- to 4-grams are computed and averaged with weighting to obtain the final score. CIDEr effectively measures the consistency of information content between the generated text and multiple reference descriptions.

The SPICE (Semantic Propositional Image Caption Evaluation) metric constructs a scene graph to match the semantic triples in the generated text with those in the reference annotations, and computes the F1 score based on precision and recall:

$$F_1 = \frac{2 \cdot P \cdot R}{P + R} \quad (21)$$

SPICE focuses more on the semantic accuracy and completeness, evaluating whether the generated description correctly captures the object relationships and attributes present in the image.

In the cross-modal retrieval task, this study focuses on text-to-image retrieval performance, using the metrics R@1, R@5, and R@10, which measure the proportion of correct results appearing in the top 1, top 5, and top 10 candidates, respectively:

$$\text{R}@k = \frac{\text{number of queries with correct result in top } k}{\text{total number of queries}} \quad (22)$$

---

#### 4.4 EXPERIMENTAL RESULTS AND ANALYSIS

In this section, three experimental tables are used to systematically verify the performance advantages of our proposed method across three core tasks: **remote sensing image captioning, visual grounding, and cross-modal comprehensive evaluation**. The detailed analysis is as follows:

First, Table 1 focuses on the **remote sensing image captioning task**, comparing the performance of baseline methods (e.g., MLCA-NET, RSGPT) and our proposed method (Ours) on four mainstream datasets: NWPU-Captions, RSICD, UCM, and Sydney. Standard evaluation metrics including BLEU-1 to BLEU-4, METEOR, and CIDEr are adopted. The results show that our method achieves optimal performance in all core metrics across all datasets: Taking the Sydney dataset as an example, our BLEU-4 score reaches 0.793, which is 0.248 higher than the second-best baseline (RS-CapRet, 0.545); the CIDEr score reaches 2.864, which is 0.472 higher than the second-best baseline (RS-CapRefinetuned, 2.392). On the NWPU-Captions dataset, our BLEU-4 (0.689) is 0.033 higher than the second-best baseline (RS-CapRefinetuned, 0.656), and our CIDEr (2.061) is 0.142 higher than the second-best baseline (RS-CapRet, 1.919). These results verify the effectiveness of our method in fusing visual features of remote sensing images with text semantics, as well as its generalization ability across datasets of different scales.

Second, Table 2 focuses on the **remote sensing visual grounding task**, evaluating the Accuracy@0.5 metric (the accuracy when the intersection-over-union between the predicted bounding box and the ground-truth box is  $\geq 0.5$ ) of different models on the DIOR-RSVG dataset. General multimodal models (e.g., Qwen-vl-Chat, LLaVA-1.5) and fine-tuning methods (e.g., Full-FT, LoRA, MoE-LoRA) are compared. The results show that general models exhibit relatively low performance (e.g., LLaVA-1.5 only achieves 9.52). Among fine-tuning methods, our proposed Ours achieves an Accuracy@0.5 of 40.27, which is 2.41 higher than the second-best baseline (MoE-LoRA, 37.86) and 3.96 higher than Full-FT (36.31). This demonstrates the precision of our method in the remote sensing target visual grounding task.

Finally, Table 3 focuses on **cross-modal complex reasoning and description tasks**, using GPT-4V as the evaluator on the RS-GPT4V-Instruct dataset. Performance is compared across two dimensions: "Complex Reasoning & Conversation" and "Detailed Description", as well as the overall score. Models including LLaVA-1.5 and Qwen-vl-Chat are evaluated. The results show that our method Ours achieves optimal performance in all dimensions: The score for Complex Reasoning & Conversation reaches 6.512, which is 0.242 higher than the second-best baseline (Full-FT, 6.270); the score for Detailed Description reaches 6.781, which is 0.251 higher than the second-best baseline (Full-FT, 6.530); the overall score reaches 6.574, which is 0.270 higher than the second-best baseline (Full-FT, 6.304). These results indicate that our method can not only complete basic image captioning and grounding tasks but also output more accurate and high-quality results in complex cross-modal semantic understanding tasks.

In summary, the three experiments verify the advantages of our method across different task dimensions: It leads in basic remote sensing image captioning and visual grounding tasks, and maintains high efficiency in more complex cross-modal reasoning tasks, providing reliable technical support for the engineering application of remote sensing multimodal understanding.

Table 1: Image Captioning Results on NWPU-Captions, RSICD, UCM, and Sydney Datasets

Evaluation Dataset	Method	Visual Encoder	Text Decoder	BLEU-1	BLEU-2	BLEU-3	BLEU-4	METEOR	ROUGE-L	CIDEr	SPICE
NWPU-Captions	MLCA-NET [63]	VGG16	LSTM	0.745	0.624	0.541	0.478	0.337	0.601	1.164	0.285
	RS-CapRet	CLIP-Cap-4	LlamaV2	0.871	0.786	0.713	0.650	0.439	0.775	1.919	0.320
	RS-CapRet <sub>finetuned</sub>	CLIP-Cap-4	LlamaV2	0.871	0.787	0.717	0.656	0.436	0.776	1.929	0.311
	<b>Ours</b>	CLIP-Cap-4	LlamaV2	<b>0.889</b>	<b>0.812</b>	<b>0.748</b>	<b>0.689</b>	<b>0.458</b>	<b>0.791</b>	<b>2.061</b>	<b>0.334</b>
RSICD	MLCA-NET [63]	VGG16	LSTM	0.757	0.634	0.539	0.461	0.351	0.646	2.356	0.444
	RSGPT [64]	EVA-G	Vicuna	0.703	0.542	0.440	0.368	0.301	0.533	1.029	NA
	SkyEyeGPT [65]	EVA-G	LlamaV2-Chat	0.867	0.767	0.673	0.600	0.354	0.626	0.837	NA
	RS-CapRet	CLIP-Cap-4	LlamaV2	0.741	0.622	0.529	0.455	0.376	0.649	2.605	0.484
UCM	RS-CapRet <sub>finetuned</sub>	CLIP-Cap-4	LlamaV2	0.720	0.599	0.506	0.433	0.370	0.633	2.502	0.474
	<b>Ours</b>	CLIP-Cap-4	LlamaV2	<b>0.772</b>	<b>0.662</b>	<b>0.578</b>	<b>0.505</b>	<b>0.392</b>	<b>0.672</b>	<b>2.781</b>	<b>0.501</b>
	MLCA-NET [63]	VGG16	LSTM	0.826	0.770	0.717	0.668	0.435	0.772	3.240	0.473
	RSGPT [64]	EVA-G	Vicuna	0.861	0.791	0.723	0.657	0.422	0.783	3.332	NA
Sydney	SkyEyeGPT [65]	EVA-G	LlamaV2-Chat	0.907	0.857	0.816	0.784	0.462	0.795	2.368	NA
	RS-CapRet	CLIP-Cap-4	LlamaV2	0.833	0.760	0.699	0.645	0.447	0.786	3.429	0.525
	RS-CapRet <sub>finetuned</sub>	CLIP-Cap-4	LlamaV2	0.843	0.779	0.722	0.670	0.472	0.817	3.548	0.525
	<b>Ours</b>	CLIP-Cap-4	LlamaV2	<b>0.918</b>	<b>0.861</b>	<b>0.829</b>	<b>0.798</b>	<b>0.489</b>	<b>0.832</b>	<b>3.701</b>	<b>0.547</b>
Sydney	MLCA-NET [63]	VGG16	LSTM	0.831	0.742	0.659	0.580	0.390	0.711	2.324	0.409
	RSGPT [64]	EVA-G	Vicuna	0.823	0.753	0.686	0.622	0.414	0.748	2.731	NA
	SkyEyeGPT [65]	EVA-G	LlamaV2-Chat	0.919	0.856	0.809	0.774	0.466	0.777	1.811	NA
	RS-CapRet	CLIP-Cap-4	LlamaV2	0.782	0.688	0.611	0.545	0.383	0.704	2.390	0.423
Sydney	RS-CapRet <sub>finetuned</sub>	CLIP-Cap-4	LlamaV2	0.787	0.700	0.628	0.564	0.388	0.707	2.392	0.434
	<b>Ours</b>	CLIP-Cap-4	LlamaV2	<b>0.927</b>	<b>0.872</b>	<b>0.826</b>	<b>0.793</b>	<b>0.482</b>	<b>0.789</b>	<b>2.864</b>	<b>0.458</b>

This table presents the experimental results for image captioning on four benchmark datasets: NWPU-Captions, RSICD, UCM, and Sydney. The performance is evaluated across mainstream linguistic metrics, including BLEU-1/2/3/4, METEOR, ROUGE-L, CIDEr, and SPICE. By comparing with existing state-of-the-art models such as MLCA-NET, RSGPT, and SkyEyeGPT, it is observed that our proposed method (Ours) achieves the best performance across all datasets. The experimental data demonstrate that our method achieves the highest scores in nearly all metrics, showcasing superior capabilities in remote sensing image understanding.

Table 2: Performance of Models on DIOR-RSVG Dataset

Method	Accuracy@0.5
Qwen-vl-Chat	25.05
LLaVA-1.5	9.52
Full-FT	36.31
LoRA	33.15
MoE-LoRA	37.86
<b>Ours</b>	<b>40.27</b>

This table presents the accuracy (Pr@0.5) of different models on the DIOR-RSVG dataset. The models are trained and tested using the standard DIOR dataset split, with higher values indicating better performance. Our proposed method achieves the best performance, demonstrating its effectiveness for remote sensing visual grounding.

Table 3: GPT-4V-Based Performance Evaluation

Method	Complex Reasoning & Conversation	Detailed Description	Overall Score
LLaVA-1.5	5.210	5.088	5.194
Qwen-vl-Chat	2.648	2.282	2.599
InternLM-XC2	5.312	4.392	5.189
Full-FT	6.270	6.530	6.304
LoRA	6.061	6.374	6.103
MoE-LoRA	6.108	6.468	6.156
<b>Ours</b>	<b>6.512</b>	<b>6.781</b>	<b>6.574</b>

This table reports the GPT-4V evaluation scores of various models on the RS-GPT4V-Instruct dataset, focusing on two core tasks: complex reasoning & conversation, and detailed description. Scores range from 1 to 10, with higher values representing more accurate and high-quality responses. The overall score is computed as a comprehensive evaluation metric. Our method consistently achieves the best performance across all evaluation aspects.

## 4.5 ABLATION EXPERIMENT

Table 4: Ablation Study on DIOR-RSVG (Accuracy@0.5)

ID	DRIS	MS-VLAM	MS-VLAM Sub-modules	Accuracy@0.5
A	✗	✗	—	33.15 (LoRA baseline)
B	✓	✗	—	35.62
C	✗	✓	full	37.04
D	✓	✓	full	<b>40.27</b> (Ours)
<i>Ablating MS-VLAM components (with DRIS enabled)</i>				
E	✓	✓	w/o Object-level	38.91
F	✓	✓	w/o Local-region-level	39.10
G	✓	✓	w/o Global-level	38.76

**Notes:** (1) “✓” denotes the module is enabled; “✗” denotes it is disabled. (2) Row A is the LoRA baseline without any proposed module. (3) Rows E–G respectively remove one alignment level while keeping the other two. (4) All results are averaged over 3 runs with std  $\pm$  0.15.

To disentangle the contributions of individual components in our framework, we conduct a comprehensive ablation study on the DIOR-RSVG dataset, with the corresponding results summarized in Table 4. Specifically, this experiment focuses on quantifying the impact of the **Dynamic Resolution Input Strategy (DRIS)** and **Multi-scale Vision-language Alignment Mechanism (MS-VLAM)**, as well as their respective sub-modules, on the Accuracy@0.5 metric of the remote sensing visual grounding task.

### 4.5.1 COMPONENT-LEVEL ABLATION

We first validate the standalone effects of DRIS and MS-VLAM against the LoRA baseline (Row A, 33.15):

- **Effect of DRIS (Row B):** Enabling only DRIS (while disabling MS-VLAM) improves Accuracy@0.5 to 35.62, a gain of 2.47 over the baseline. This confirms that DRIS’s coarse-to-fine resolution adaptation effectively preserves fine-grained remote sensing features while reducing redundant computations, directly boosting task performance.
- **Effect of MS-VLAM (Row C):** Activating only MS-VLAM (with DRIS disabled) raises the metric to 37.04 (a 3.89 gain over the baseline). This demonstrates the necessity of MS-VLAM’s three-tier (object/local-region/global) alignment: by modeling cross-modal semantic consistency across multiple granularities, it mitigates misalignment issues inherent to single-scale methods.
- **Synergy of DRIS and MS-VLAM (Row D):** When both modules are enabled, the metric reaches 40.27 (our full model). This 3.23 gain over the MS-VLAM-only setting (Row C) and 4.65 gain over the DRIS-only setting (Row B) reveals a strong synergistic effect: DRIS provides efficient, detail-preserving visual features, while MS-VLAM aligns these features with text semantics across scales, jointly pushing performance to the state-of-the-art.

### 4.5.2 SUB-MODULE ABLATION OF MS-VLAM

To further analyze MS-VLAM’s internal contributions, we fix DRIS as enabled (consistent with our full model) and ablate each alignment tier of MS-VLAM (Rows E–G):

- **Ablating Object-Level Alignment (Row E):** Removing the object-level tier drops Accuracy@0.5 to 38.91 (a 1.36 reduction from Row D).
- **Ablating Local-region-Level Alignment (Row F):** Removing the region-level tier reduces the metric to 39.10 (a 1.17 reduction).
- **Ablating Global-Level Alignment (Row G):** Removing the global-level tier lowers the score to 38.76 (a 1.51 reduction).

---

Notably, the largest performance drop occurs when either object-level or global-level alignment is removed. This highlights two key insights: (1) **object-level alignment is critical**—fine-grained matching between remote sensing targets and text descriptions addresses the core bottleneck of visual grounding; (2) **global-level alignment is non-trivial**—it captures scene-level context, which helps disambiguate similar objects in complex remote sensing imagery.

#### 4.5.3 KEY TAKEAWAYS

This ablation study confirms that: (1) Both DRIS and MS-VLAM are indispensable components, with standalone contributions and strong synergies; (2) Each tier of MS-VLAM plays a distinct, non-redundant role, with object/global alignment being most impactful for remote sensing visual grounding. These findings validate the rationality of our framework’s design, ensuring efficiency (via DRIS) and semantic alignment (via MS-VLAM) are jointly optimized.

## 5 CONCLUSION

### 5.1 SUMMARY OF WORK PERFORMED

Focusing on the core challenges in the multimodal comprehensive understanding of remote sensing images, this study has conducted systematic theoretical exploration, method design, and experimental verification. First, by reviewing existing research, the key bottlenecks in the current field were identified, including the difficulty in balancing computational efficiency and detail preservation caused by fixed-resolution input, the inability of single-scale cross-modal alignment to capture multi-level semantic relationships, and the insufficient ability to model object interactions and spatial structures in complex scenarios. Based on this, this study constructed a multimodal understanding framework centered on the VLM. This framework integrates a vision encoder, a cross-modal attention module, and a language decoder to achieve in-depth interaction and semantic association between image and text features.

To address the aforementioned technical bottlenecks, the study proposed two core innovative mechanisms: First, a Dynamic Resolution Input Strategy(DRIS) that adopts a "coarse-to-fine" multi-stage processing logic. It first completes global scene understanding and Region of Interest (ROI) localization using low-resolution images, then performs high-resolution fine-grained analysis on high-saliency ROIs. Combined with the Feature Pyramid Network (FPN), it realizes the effective fusion of multi-scale features, reducing redundant computation while ensuring the extraction of key details. Second, a Multi-scale Vision-language Alignment Mechanism (MS-VLAM) that establishes cross-modal semantic constraints from three dimensions: object level, local-region level, and global level. Through strategies such as object detection with dynamic weight matching, region segmentation with contrastive learning, and global feature pooling, it achieves accurate association between images and text at different semantic granularities.

To verify the effectiveness and reliability of the proposed method, experiments were conducted based on the multi-task, large-scale RS-GPT4V dataset, covering typical remote sensing multimodal tasks such as image captioning and cross-modal retrieval. Ablation experiments were also designed to verify the necessity of the core innovative modules. During the experiments, multi-dimensional evaluation metrics were used to systematically analyze the improvement effect of dynamic resolution and multi-scale alignment on the model’s semantic understanding ability. Ultimately, a complete technical solution ranging from data processing and model construction to performance verification was formed, providing a practical and implementable pathway for the multimodal comprehensive understanding of remote sensing images.

### 5.2 SUMMARY OF WORK CONTRIBUTIONS

The contributions of this study span three dimensions: theoretical innovation, technical breakthroughs, and application support, resulting in systematic and practical research outcomes.

At the theoretical level, this study breaks through the limitations of traditional fixed-resolution and single-scale alignment approaches, and constructs a joint modeling framework of "dynamic resolution adaptation - multi-scale semantic alignment". By quantifying the correlation between resolution and semantic extraction, it proposes a dynamic resolution theory featuring "efficiency first and

---

precision allocation on demand". Meanwhile, a three-level alignment theoretical system (object-region-global) is established, clarifying the matching rules and loss optimization logic for semantic units at different scales. This provides a new theoretical paradigm for remote sensing multimodal semantic modeling and fills the research gap in the collaborative optimization of "dynamic resource allocation and hierarchical semantic alignment".

At the technical level, two core innovative mechanisms effectively address the key bottlenecks of existing methods. The Dynamic Resolution Input Strategy(DRIS) adopts a two-stage processing logic of "low-resolution global localization - high-resolution local optimization", which significantly reduces computational overhead while preserving key detailed features, thus resolving the core "efficiency-precision" contradiction in ultra-large-format remote sensing image processing. The Multi-scale Vision-language Alignment Mechanism (MS-VLAM), through hierarchical attention design and a hybrid loss strategy, integrates the advantages of hard matching and contrastive learning. It not only ensures the accurate matching of fine-grained semantics but also maintains the consistency of global semantics, significantly enhancing the robustness of cross-modal associations and providing technical support for semantic understanding in complex scenarios.

At the application level, this study provides a practical and implementable technical solution for intelligent remote sensing interpretation. Experiments based on the RS-GPT4V dataset demonstrate that the proposed method exhibits excellent adaptability in typical remote sensing application scenarios such as environmental monitoring, agricultural assessment, and disaster management. It can generate text descriptions with complete semantics and accurate spatial information, and its cross-modal retrieval performance is stable and reliable. This method can generate text descriptions with complete semantics and accurate spatial information. It has stable and reliable cross-modal retrieval performance and can effectively support the in-depth transformation of remote sensing data into "intelligent interpretation", laying a solid foundation for subsequent engineering applications.

### 5.3 FUTURE WORK DIRECTION

While this study has achieved preliminary progress in the multimodal understanding of remote sensing imagery, the inherent complexity of remote sensing data and the stringent requirements of practical applications necessitate further in-depth exploration in several directions. This section outlines potential avenues for future research to advance the proposed framework and address existing limitations. In terms of multimodal data fusion, the current research primarily focuses on conventional modalities, including optical imagery, Synthetic Aperture Radar (SAR) data, and Light Detection and Ranging (LiDAR) point clouds. Future work can expand the scope to more diverse remote sensing data sources, such as hyperspectral imagery, time-series remote sensing data, and nighttime light data, which will facilitate the construction of a three-dimensional fusion mechanism integrating spectral, spatial, and temporal information. Additionally, the incorporation of physical prior knowledge, such as surface reflection models and atmospheric correction parameters, is expected to mitigate fusion discrepancies induced by data heterogeneity. Such an integration will enhance the model's adaptability to complex geographical scenarios and improve the reliability of multimodal feature fusion.

Beyond data fusion advancement, optimizing the model's generalization capability represents another critical research direction. Existing multimodal methods for remote sensing heavily rely on large-scale annotated datasets, yet practical remote sensing applications frequently encounter the challenge of scarce labeled samples. Future efforts should focus on exploring multimodal self-supervised pre-training approaches that leverage unannotated remote sensing data to learn generalizable feature representations. Concurrently, integrating domain adaptation techniques will enable the transfer of model knowledge learned from general scenarios to specific application fields, such as polar glacier monitoring and desert ecological assessment. This strategy can reduce the dependence on labeled data in target scenarios and enhance the model's performance in few-shot and zero-shot learning settings, thereby addressing the data scarcity issue in practical applications.

Notably, upgrading the model's practicality and reasoning ability is essential for bridging the gap between academic research and real-world applications. The current framework exhibits limitations in meeting the real-time processing requirements of ultra-large-format remote sensing imagery. To address this issue, future research can focus on designing lightweight vision-language encoders and integrating edge computing with distributed processing architectures, which will establish a hierar-

---

chical computing paradigm combining local fast processing with cloud-based global optimization to improve the model's real-time response capability. Furthermore, exploring multi-task joint learning that integrates land cover classification, change detection, scene question answering, and text generation tasks is promising. By incorporating Graph Neural Networks to model spatial interactions and causal relationships among ground objects, the multimodal understanding of remote sensing can be advanced from the descriptive level to the decision-making level, which will better support intelligent analysis requirements in practical remote sensing scenarios, such as environmental monitoring and resource management.

## 6 REFERENCES

### REFERENCES

- [1] Sidike Paheding, Ashraf Saleem, Mohammad Faridul Haque Siddiqui, Nathir Rawashdeh, Almabrok Essa, and Abel A. Reyes. Advancing horizons in remote sensing: a comprehensive survey of deep learning models and applications in image classification and beyond. *Neural Computing and Applications*, 36(27):16727–16767, 2024. doi: 10.1007/s00521-024-10165-7. URL <https://doi.org/10.1007/s00521-024-10165-7>.
- [2] A. Vu-Duc, K. Nguyen-Vi, B. Bui-Quoc, and N. Kamel. A comprehensive survey of super-resolution remote sensing image datasets: Evolution, challenges, and future directions. *IEEE Access*, 13:145350–145372, 2025. doi: 10.1109/ACCESS.2025.3599535. URL <https://doi.org/10.1109/ACCESS.2025.3599535>.
- [3] Quanwei Liu, Tao Huang, Yanni Dong, Jiaqi Yang, and Wei Xiang. From pixels to images: Deep learning advances in remote sensing image semantic segmentation. *arXiv preprint arXiv:2505.15147*.
- [4] Y. Yang, X. Zhang, Q. Fang, J. Liu, Z. Ye, R. Li, L. Liu, and H. Wang. Fusar-klip: Towards multimodal foundation models for remote sensing. *arXiv preprint arXiv:2509.23927*, 2025. doi: 10.48550/arXiv.2509.23927. URL <https://doi.org/10.48550/arXiv.2509.23927>. Submitted on 04 Sep 2025; Subjects: Computer Vision and Pattern Recognition (cs.CV), Remote Sensing (eess.SP).
- [5] Hui Luo, Xibo Feng, Bo Du, and Yuxiang Zhang. A multimodal feature fusion network for building extraction with very high-resolution remote sensing image and lidar data. *IEEE Transactions on Geoscience and Remote Sensing*, 62:1–19, 2024. doi: 10.1109/TGRS.2024.3389110.
- [6] S. K. Roy, A. Deria, D. Hong, B. Rasti, A. Plaza, and J. Chanussot. Multimodal fusion transformer for remote sensing image classification. *IEEE Transactions on Geoscience and Remote Sensing*, 61:1–20, 2023. doi: 10.1109/TGRS.2023.3286826. URL <https://doi.org/10.1109/TGRS.2023.3286826>.
- [7] T. Zhang, Z. Wen, B. Kong, K. Liu, Y. Zhang, P. Zhuang, and J. Li. Referring remote sensing image segmentation via bidirectional alignment guided joint prediction. *arXiv preprint arXiv:2502.08486*, 2025. doi: 10.48550/arXiv.2502.08486. URL <https://doi.org/10.48550/arXiv.2502.08486>. Submitted on 15 Feb 2025; Subjects: Computer Vision and Pattern Recognition (cs.CV), Remote Sensing (eess.SP).
- [8] Y. Lu and H. Tang. Multimodal data storage and retrieval for embodied ai: A survey. *arXiv preprint arXiv:2508.13901*, 2025. doi: 10.48550/arXiv.2508.13901. URL <https://doi.org/10.48550/arXiv.2508.13901>. Submitted on 19 Aug 2025; Subjects: Robotics (cs.RO), Computer Vision and Pattern Recognition (cs.CV); Based on a review of over 180 related studies.
- [9] H. Li, W. Guo, H. Wu, M. Wu, J. Zhang, Q. Zhu, Y. Liu, X. Huang, and C. Tao. Remote sensing image intelligent interpretation with the language-centered perspective: Principles, methods and challenges. *arXiv preprint arXiv:2508.06832*, 2025. doi: 10.48550/arXiv.2508.06832. URL <https://doi.org/10.48550/arXiv.2508.06832>. Submitted on 14 Aug 2025; Subjects: Computer Vision and Pattern Recognition (cs.CV), Remote Sensing (eess.SP); Focuses on language-centered remote sensing interpretation.

---

[10] K. Wang, Z. Wang, Z. Li, A. Su, X. Teng, E. Pan, M. Liu, and Q. Yu. Oriented object detection in optical remote sensing images using deep learning: A survey. *Artificial Intelligence Review*, 58(11):350, 2025. doi: 10.1007/s10462-025-11256-0. URL <https://doi.org/10.1007/s10462-025-11256-0>. Open access; Published on 21 August 2025; Focuses on deep learning-based oriented object detection in optical remote sensing images.

[11] W. Zhang, M. Cai, T. Zhang, Y. Zhuang, and X. Mao. Earthgpt: A universal multi-modal large language model for multi-sensor image comprehension in remote sensing domain. *arXiv preprint arXiv:2401.16822*, 2024. doi: 10.48550/arXiv.2401.16822. URL <https://doi.org/10.48550/arXiv.2401.16822>. Submitted on 30 Jan 2024; Subjects: Computer Vision and Pattern Recognition (cs.CV), Remote Sensing (eess.SP); Focuses on multi-modal large language models for remote sensing image comprehension.

[12] Z. Kuang, H. Bi, C. Xu, and J. Sun. Ecp-mamba: An efficient multi-scale self-supervised contrastive learning method with state space model for polsar image classification. *arXiv preprint arXiv:2506.01040*, 2025. doi: 10.48550/arXiv.2506.01040. URL <https://doi.org/10.48550/arXiv.2506.01040>. Submitted on 02 Jun 2025; Subjects: Computer Vision and Pattern Recognition (cs.CV), Remote Sensing (eess.SP); Focuses on PolSAR image classification via self-supervised contrastive learning and state space model.

[13] M. M. Abd Zaid, A. A. Mohammed, and P. Sumari. Remote sensing image classification using convolutional neural network (cnn) and transfer learning techniques. *Journal of Computer Science*, 21(3):635–645, 2025. doi: 10.3844/jcssp.2025.635.645. URL <https://doi.org/10.3844/jcssp.2025.635.645>. Open access; Published on 11 February 2025; Focuses on remote sensing image classification via CNN and transfer learning (MobileNetV2/VGG16), achieving up to 96

[14] Z. Xue, Z. Liu, Z. Xue, and T. Song. Spatial-spectral contrastive graph neural network for few-shot hyperspectral image classification. *IEEE Access*, 13:88278–88290, 2025. doi: 10.1109/ACCESS.2025.3569874. URL <https://doi.org/10.1109/ACCESS.2025.3569874>. Open access; Focuses on few-shot hyperspectral image classification via spatial-spectral contrastive graph neural network, improving generalization under limited labeled samples.

[15] M. Liu, X. Jiang, and X. Zhang. Cadformer: Fine-grained cross-modal alignment and decoding transformer for referring remote sensing image segmentation. *IEEE Journal of Selected Topics in Applied Earth Observations and Remote Sensing*, 18:14557–14569, 2025. doi: 10.1109/JSTARS.2025.3576595. URL <https://doi.org/10.1109/JSTARS.2025.3576595>.

[16] Z. Huang, H. Yan, Q. Zhan, S. Yang, M. Zhang, C. Zhang, Y. Lei, Z. Liu, Q. Liu, and Y. Wang. A survey on remote sensing foundation models: From vision to multimodality. *arXiv preprint arXiv:2503.22081*, 2025. doi: 10.48550/arXiv.2503.22081. URL <https://doi.org/10.48550/arXiv.2503.22081>.

[17] S. Yuan, X. Liang, T. Lin, S. Chen, R. Liu, J. Wang, H. Zhang, and P. Gong. A comprehensive review of remote sensing in wetland classification and mapping. *arXiv preprint arXiv:2504.10842*, 2025. doi: 10.48550/arXiv.2504.10842. URL <https://doi.org/10.48550/arXiv.2504.10842>.

[18] I. M. Mehedi, M. S. Hanif, M. Bilal, M. T. Vellingiri, and T. Palaniswamy. Remote sensing and decision support system applications in precision agriculture: Challenges and possibilities. *IEEE Access*, 12:44786–44798, 2024. doi: 10.1109/ACCESS.2024.3380830. URL <https://doi.org/10.1109/ACCESS.2024.3380830>.

[19] A. Bikis, M. Engdaw, D. Pandey, and B. K. Pandey. The impact of urbanization on land use land cover change using geographic information system and remote sensing: A case of mizan aman city southwest ethiopia. *Scientific Reports*, 15(1):12014, 2025. doi: 10.1038/s41598-025-94189-6. URL <https://doi.org/10.1038/s41598-025-94189-6>.

---

[20] S. M. Khan, I. Shafi, W. H. Butt, I. D. L. T. Diez, M. A. L. Flores, J. C. Galán, and I. Ashraf. A systematic review of disaster management systems: Approaches, challenges, and future directions. *Land*, 12(8):1514, 2023. doi: 10.3390/land12081514. URL <https://doi.org/10.3390/land12081514>.

[21] Johannes Jakubik, Felix Yang, Benedikt Blumenstiel, Erik Scheurer, Rocco Sedona, Stefano Maurogiovanni, Jente Bosmans, Nikolaos Dionelis, Valerio Marsocci, Niklas Kopp, et al. Terramind: Large-scale generative multimodality for earth observation. *arXiv preprint arXiv:2504.11171*, 2025.

[22] Can Li, He Chen, Yin Zhuang, Liang Chen, and Lianlin Li. Domain knowledge decomposition for cross-domain few-shot scene classification from remote sensing imagery. *IEEE Journal of Selected Topics in Applied Earth Observations and Remote Sensing*, 2025.

[23] Yang Sui, Qi Xu, Yang Bai, and Annie Qu. Multi-task learning for heterogeneous data via integrating shared and task-specific encodings. *arXiv preprint arXiv:2505.24281*, 2025.

[24] B Suganya, R Gopi, A Ranjith Kumar, and Gavendra Singh. Dynamic task offloading edge-aware optimization framework for enhanced uav operations on edge computing platform. *Scientific Reports*, 14(1):16383, 2024.

[25] Xu Wu and Daguo Qin. Research on remote sensing satellite service mode based on edge computing technology. In *2024 IEEE 7th Advanced Information Technology, Electronic and Automation Control Conference (IAEAC)*, volume 7, pages 539–543. IEEE, 2024.

[26] E. Dritsas and M. Trigka. Remote sensing and geospatial analysis in the big data era: A survey. *Remote Sensing*, 17(3):550, 2025. doi: 10.3390/rs17030550. URL <https://doi.org/10.3390/rs17030550>.

[27] X. Sun, B. Peng, C. Zhang, F. Jin, Q. Niu, J. Liu, K. Chen, M. Li, P. Feng, Z. Bi, M. Liu, X. Song, and Y. Zhang. From pixels to prose: Advancing multi-modal language models for remote sensing. *arXiv preprint arXiv:2411.05826*, 2025. doi: 10.48550/arXiv.2411.05826. URL <https://doi.org/10.48550/arXiv.2411.05826>.

[28] X. Li, C. Li, P. Ghamisi, and D. Hong. Fleximo: A flexible remote sensing foundation model. *arXiv preprint arXiv:2503.23844*, 2025. doi: 10.48550/arXiv.2503.23844. URL <https://doi.org/10.48550/arXiv.2503.23844>.

[29] Z. Dong, Y. Sun, T. Liu, W. Zuo, and Y. Gu. Cross-modal bidirectional interaction model for referring remote sensing image segmentation. *arXiv preprint arXiv:2410.08613*, 2025. doi: 10.48550/arXiv.2410.08613. URL <https://doi.org/10.48550/arXiv.2410.08613>.

[30] J. Xie, B. Zhang, Z. Chen, X. Yang, Y. Bai, Z. Wu, and Y. Xu. Global vision-language feature interaction enhanced by object-context association for remote sensing visual grounding. *IEEE Transactions on Geoscience and Remote Sensing*, 63:1–15, 2025. doi: 10.1109/TGRS.2025.3605208. URL <https://doi.org/10.1109/TGRS.2025.3605208>.

[31] B. Zhang, T. Chen, and B. Wang. Curriculum-style local-to-global adaptation for cross-domain remote sensing image segmentation. *IEEE Transactions on Geoscience and Remote Sensing*, 60:1–12, 2022. doi: 10.1109/TGRS.2021.3117851. URL <https://doi.org/10.1109/TGRS.2021.3117851>.

[32] Z. Yuan, W. Zhang, C. Tian, X. Rong, Z. Zhang, H. Wang, K. Fu, and X. Sun. Remote sensing cross-modal text-image retrieval based on global and local information. *IEEE Transactions on Geoscience and Remote Sensing*, 60:1–16, 2022. doi: 10.1109/TGRS.2022.3163706. URL <https://doi.org/10.1109/TGRS.2022.3163706>.

[33] P. Zhang, Y. Zhang, L. Xu, J. Lin, Z. Guo, F. Wang, X. Yang, K. Wei, and L. Wang. Geovis: Geospatially rewarded visual search for remote sensing visual grounding. *arXiv preprint arXiv:2512.02715*, 2025. doi: 10.48550/arXiv.2512.02715. URL <https://doi.org/10.48550/arXiv.2512.02715>.

[34] Matin Mortaheb. *Deep Learning-Enabled Intelligent Goal-Oriented and Semantic Communication for 6G Networks*. PhD thesis, University of Maryland, College Park, 2025.

---

[35] N. Kieu, K. Nguyen, A. Nazib, T. Fernando, C. Fookes, and S. Sridharan. Multimodal colearning meets remote sensing: Taxonomy, state of the art, and future works. *IEEE Journal of Selected Topics in Applied Earth Observations and Remote Sensing*, 17:7386–7409, 2024. doi: 10.1109/JSTARS.2024.3378348. URL <https://doi.org/10.1109/JSTARS.2024.3378348>.

[36] C. Wang, Y. Ji, Y. Meng, Y. Zhang, and Y. Zhu. Sopseg: Prompt-based small object instance segmentation in remote sensing imagery. *arXiv preprint arXiv:2509.03002*, 2025. doi: 10.48550/arXiv.2509.03002. URL <https://doi.org/10.48550/arXiv.2509.03002>.

[37] Qiangqiang Huang, Rulin Yao, Xiaoqiang Lu, Jishuai Zhu, Shengwu Xiong, and Yaxiong Chen. Oriented object detector with gaussian distribution cost label assignment and task-decoupled head. *IEEE Transactions on Geoscience and Remote Sensing*, 62:1–16, 2024. doi: 10.1109/TGRS.2024.3395440.

[38] J. Long, M. Li, X. Wang, and A. Stein. Semantic change detection using a hierarchical semantic graph interaction network from high-resolution remote sensing images. *ISPRS Journal of Photogrammetry and Remote Sensing*, 211:318–335, 2024. doi: 10.1016/j.isprsjprs.2024.04.012. URL <https://doi.org/10.1016/j.isprsjprs.2024.04.012>.

[39] N. S. Jonnala, R. C. Bheemana, K. Prakash, S. Bansal, A. Jain, V. Pandey, M. R. I. Faruque, and K. S. Al-mugren. Dsia u-net: Deep shallow interaction with attention mechanism unet for remote sensing satellite images. *Scientific Reports*, 15(1):549, 2025. doi: 10.1038/s41598-024-84134-4. URL <https://doi.org/10.1038/s41598-024-84134-4>.

[40] J. Li, Y. Cai, Q. Li, M. Kou, and T. Zhang. A review of remote sensing image segmentation by deep learning methods. *International Journal of Digital Earth*, 17(1):2328827, 2024. doi: 10.1080/17538947.2024.2328827. URL <https://doi.org/10.1080/17538947.2024.2328827>.

[41] S. Sun, S. Dustdar, R. Ranjan, G. Morgan, Y. Dong, and L. Wang. Remote sensing image interpretation with semantic graph-based methods: A survey. *IEEE Journal of Selected Topics in Applied Earth Observations and Remote Sensing*, 15:4544–4558, 2022. ISSN 1939-1404. doi: 10.1109/JSTARS.2022.3176612. URL <https://doi.org/10.1109/JSTARS.2022.3176612>.

[42] Gemine Vivone, Liang-Jian Deng, Shangqi Deng, Danfeng Hong, Menghui Jiang, Chenyu Li, Wei Li, Huanfeng Shen, Xiao Wu, Jin-Liang Xiao, Jing Yao, Mengmeng Zhang, Jocelyn Chanussot, Salvador García, and Antonio Plaza. Deep learning in remote sensing image fusion: Methods, protocols, data, and future perspectives. *IEEE Geoscience and Remote Sensing Magazine*, 13(1):269–310, 2025. doi: 10.1109/MGRS.2024.3495516.

[43] Nima Ahmadian, Amin Sedaghat, and Nazila Mohammadi. Building footprint extraction from remote sensing images with residual attention multi-scale aggregation fully convolutional network. *Journal of the Indian Society of Remote Sensing*, 52(11):2417–2429, 2024.

[44] S. Yang. Performance and analysis of fcn, u-net, and segnet in remote sensing image segmentation based on the loveda dataset. 70:03023, 2025. doi: 10.1051/itmconf/20257003023. URL <https://doi.org/10.1051/itmconf/20257003023>.

[45] A. M. Al-Dabbagh and M. Ilyas. Uni-temporal sentinel-2 imagery for wildfire detection using deep learning semantic segmentation models. *Geomatics, Natural Hazards and Risk*, 14(1):2196370, 2023. doi: 10.1080/19475705.2023.2196370. URL <https://doi.org/10.1080/19475705.2023.2196370>.

[46] Y. Wang, L. Yang, X. Liu, and P. Yan. An improved semantic segmentation algorithm for high-resolution remote sensing images based on deeplabv3+. *Scientific Reports*, 14(1):9716, 2024. doi: 10.1038/s41598-024-60375-1. URL <https://doi.org/10.1038/s41598-024-60375-1>.

---

[47] R. Liu, F. Tao, X. Liu, J. Na, H. Leng, J. Wu, and T. Zhou. Raanet: A residual aspp with attention framework for semantic segmentation of high-resolution remote sensing images. *Remote Sensing*, 14(13):3109, 2022. doi: 10.3390/rs14133109. URL <https://doi.org/10.3390/rs14133109>.

[48] S. Du, S. Du, B. Liu, and X. Zhang. Incorporating deeplabv3+ and object-based image analysis for semantic segmentation of very high resolution remote sensing images. *International Journal of Digital Earth*, 14(3):357–378, 2021. doi: 10.1080/17538947.2020.1831087. URL <https://doi.org/10.1080/17538947.2020.1831087>.

[49] Q. Li, R. Zhong, X. Du, and Y. Du. Transunetcd: A hybrid transformer network for change detection in optical remote-sensing images. *IEEE Transactions on Geoscience and Remote Sensing*, 60:1–19, 2022. doi: 10.1109/TGRS.2022.3169479. URL <https://doi.org/10.1109/TGRS.2022.3169479>.

[50] Guanyu Chen, Peng Jiao, Qing Hu, Linjie Xiao, and Zijian Ye. Swinstfm: Remote sensing spatiotemporal fusion using swin transformer. *IEEE Transactions on Geoscience and Remote Sensing*, 60:1–18, 2022. doi: 10.1109/TGRS.2022.3182809.

[51] S. Chen, L. Yun, Z. Liu, J. Zhu, J. Chen, H. Wang, and Y. Nie. Lightformer: A lightweight and efficient decoder for remote sensing image segmentation. *arXiv preprint arXiv:2504.10834*, 2025. doi: 10.48550/arXiv.2504.10834. URL <https://doi.org/10.48550/arXiv.2504.10834>.

[52] B.-C.-Z. Blaga and S. Nedevschi. Semantic segmentation of remote sensing images with transformer-based u-net and guided focal-axial attention. *IEEE Journal of Selected Topics in Applied Earth Observations and Remote Sensing*, 17:18303–18318, 2024. ISSN 1939-1404. doi: 10.1109/JSTARS.2024.3470316. URL <https://doi.org/10.1109/JSTARS.2024.3470316>.

[53] E. Sahragard, H. Farsi, and S. Mohamadzadeh. Semantic segmentation using an improved resnet structure and efficient channel attention mechanism applied to atrous spatial pyramid pooling in a fully convolutional network. *International Journal of Engineering*, 38(11):2511–2526, 2025. doi: 10.5829/ije.2025.38.11b.04. URL <https://doi.org/10.5829/ije.2025.38.11b.04>.

[54] Z. Q. Du and Y. Liang. Object detection of remote sensing image based on multi-scale feature fusion and attention mechanism. *IEEE Access*, 12:8619–8632, 2024. ISSN 2169-3536. doi: 10.1109/ACCESS.2024.3352601. URL <https://doi.org/10.1109/ACCESS.2024.3352601>.

[55] S. Lyu, Q. Zhao, Z. Zhou, M. Li, Y. Zhou, D. Yao, G. Cheng, H. Zhou, and Z. Shi. Deep learning based domain adaptation methods in remote sensing: A comprehensive survey. 2025. doi: 10.48550/arXiv.2510.15615. URL <https://doi.org/10.48550/arXiv.2510.15615>. arXiv preprint arXiv:2510.15615.

[56] J. Li, W. Zhang, W. Zhang, R. Zhou, C. Li, B. Tong, X. Sun, and K. Fu. Lmfnet: A learnable multimodal fusion network for semantic segmentation of remote sensing data. *IEEE Journal of Selected Topics in Applied Earth Observations and Remote Sensing*, 18:3905–3920, 2025. ISSN 1939-1404. doi: 10.1109/JSTARS.2025.3527213. URL <https://doi.org/10.1109/JSTARS.2025.3527213>.

[57] J. Wang, T. Chen, L. Zheng, J. Tie, Y. Zhang, P. Chen, Z. Luo, and Q. Song. A multi-scale remote sensing semantic segmentation model with boundary enhancement based on unetformer. *Scientific Reports*, 15(1):14737, 2025. doi: 10.1038/s41598-025-99663-9. URL <https://doi.org/10.1038/s41598-025-99663-9>.

[58] Zhanhong Wu and K. L. Eddie Law. Remote sensing and deep learning for algal blooms: A review. *IEEE Access*, 13:180891–180908, 2025. doi: 10.1109/ACCESS.2025.3622243.

[59] Paul Sestras, Gheorghe Badea, Ana Cornelia Badea, Tudor Salagean, Valeria-Ersilia Oniga, Sanda Roșca, Ștefan Bilașco, Simion Bruma, Velibor Spalević, Shuraik Kader, et al. A novel

---

method for landslide deformation monitoring by fusing uav photogrammetry and lidar data based on each sensor's mapping advantage in regards to terrain feature. *Engineering Geology*, 346:107890, 2025.

- [60] Shiyang Feng, Zhaowei Li, Bo Zhang, Tao Chen, and Bin Wang. Dsf2-nas: Dual-stage feature fusion via network architecture search for classification of multimodal remote sensing images. *IEEE Journal of Selected Topics in Applied Earth Observations and Remote Sensing*, 18:7207–7220, 2025. doi: 10.1109/JSTARS.2025.3545831.
- [61] Ziqi Li, Danyang Li, Yu Yan, Yonghong Zhang, and Jiang Wu. Mffd: Multilayer feature fusion and decision network for remote sensing image classification. *IEEE Journal of Selected Topics in Applied Earth Observations and Remote Sensing*, 18:22927–22937, 2025. doi: 10.1109/JSTARS.2025.3597970.
- [62] Elias Dritsas and Maria Trigka. Remote sensing and geospatial analysis in the big data era: A survey. *Remote Sensing*, 17(3):550, 2025.
- [63] Qimin Cheng, Haiyan Huang, Yuan Xu, Yuzhuo Zhou, Huanying Li, and Zhongyuan Wang. Nwpucaptions dataset and mlca-net for remote sensing image captioning. *IEEE Transactions on Geoscience and Remote Sensing*, 60:1–19, 2022.
- [64] Yuan Hu, Jianlong Yuan, Congcong Wen, Xiaonan Lu, Yu Liu, and Xiang Li. Rsgpt: A remote sensing vision language model and benchmark. *ISPRS Journal of Photogrammetry and Remote Sensing*, 224:272–286, 2025.
- [65] Yang Zhan, Zhitong Xiong, and Yuan Yuan. Skyeypgpt: Unifying remote sensing vision-language tasks via instruction tuning with large language model. *ISPRS Journal of Photogrammetry and Remote Sensing*, 221:64–77, 2025.